Westinghouse Non-Proprietary Class 3

WCAP-15987-NP
Revision 2

May 2003

Technical Basis for the Embedded Flaw Process for Repair of Reactor Vessel Head Penetrations

WCAP-15987-NP
Revision 2

Technical Basis for the Embedded Flaw Process for Repair of Reactor Vessel Head Penetrations

W. H. Bamford
J. P. Lareau
D. C. Adamonis
R. E. Gold
W. R. Gahwiller
P. Kreitman
C. K. Ng

May 2003

Reviewer: J. T. Crane
J. T. Crane
Regulatory and Licensing Engineering

Approved: E. A. Siegel
E. A. Siegel, Manager
Alloy 600 Product Line

Westinghouse Electric Company LLC
P.O. Box 355
Pittsburgh, PA 15230-0355

TABLE OF CONTENTS

LIST OF TABLES

LIST OF FIGURES

1 BACKGROUND AND INTRODUCTION

1.1 SUMMARY OF TECHNICAL BASIS FOR THE EMBEDDED FLAW REPAIR

The embedded flaw repair technique was developed by Westinghouse in 1994, and involves the deposition of at least three layers of Alloy 52 weld metal to isolate existing flaws and susceptible material from the primary water environment.

The embedded flaw repair technique is considered a permanent repair for a number of reasons. As long as a Primary Water Stress Corrosion Crack (PWSCC) remains isolated from the primary water (PW) environment, it cannot propagate. Since Alloy 52 weldment is resistant to PWSCC, a new PWSCC crack should not initiate and grow through the Alloy 52 overlay to permit the PW environment to contact the susceptible material. The resistance of Alloy 690 and its associated welds, Alloys 52 and 152, has been demonstrated by laboratory testing in which no cracking has been observed in simulated PWR environments, and by approximately 10 years of operational service in steam generator tubes, where no PWSCC has occurred. The crack growth resistance of this material has been documented in EPRI Report TR-109136, "Crack Growth and Microstructural Characterization of Alloy 600 PWR Vessel Head Penetration Materials," [1] and other papers. The service experience will be further discussed in Section 4.

The residual stresses produced by the embedded flaw technique have been measured and found to be relatively low [2] because of the small thickness of the weld. This implies that no new cracks will initiate and grow in the area adjacent to the repair weld. There are no other known mechanisms for significant crack propagation in this region because the cyclic fatigue loading is considered negligible. Cumulative Usage Factor (CUF) in the upper head region was calculated to be typically less than 0.2 [3] in the reactor vessel design report, as well as in various aging management review reports.

The thermal expansion properties of Alloy 52 weld metal are not specified in the ASME code, as is the case for other weld metals. In this case, the properties of the equivalent base metal (Alloy 690) should be used. For that material, the thermal expansion coefficient at 600°F is 8.2 E-6 in/in/degree F as found in Section II Part D. The Alloy 600 base metal has a coefficient of thermal expansion of 7.8 E-6 in/in/degree F, a difference of about 5 percent.

The effect of this small difference in thermal expansion is that the weld metal will contract more than the base metal when it cools, thus producing a compressive stress on the Alloy 600 tube or the attachment weld, where the crack may be located. This effect has already been accounted for in the residual stress measurements reported in the technical basis for the embedded flaw repair.

The small residual stress produced by the embedded flaw weld will act constantly, and therefore, should have no impact on the fatigue effects in the CRDM region. Since the stress would be additive to the maximum as well as the minimum stress, the stress range would not change, and the already negligible usage factor, noted above, for the region would not change at all.

1.2 DISCUSSION OF GEOMETRY

The embedded flaw repair technique is intended for application to reactor vessel head penetrations designed by Westinghouse and Combustion Engineering. The CRDM and CEDM tubes have similar geometries, with an outer diameter ranging from 3.50 to 4.25 inches for CEDMs, and a constant outer diameter of 4.0 inches for CRDMs. The ID of the CEDMs ranges from 2.718 to 2.728 inches, while the CRDMs have a constant inside diameter of 2.75 inches. Most Combustion Engineering designs also have incore instrumentation (ICI) penetrations in the upper head regions. The OD of the ICI penetrations ranges from 4.5 inches to 6.625 inches. The ID of these tubes ranges from 3.625 to 5.19 inches.

The embedded flaw repair for a head penetration is shown schematically in Figure 1-1. Notice that the inside diameter must be maintained after repair to allow for travel of the CRDMs or CEDMs.

The repair for a J-weld is shown schematically in Figure 1-2, where it can be seen that no excavation is required in this case. The extent of the repair weld is such that the entire Alloy 182/82 weld is covered, as will be discussed in Section 2 of the report.

Notes

Revision 1 of this report was prepared to provide some minor clarifications, which are, marked in the margin.

Revision 2 of this report added Appendix C, which provides an analytical basis for the embedded flaw repair, documenting the size flaws which can be embedded, while maintaining the ASME code margins.

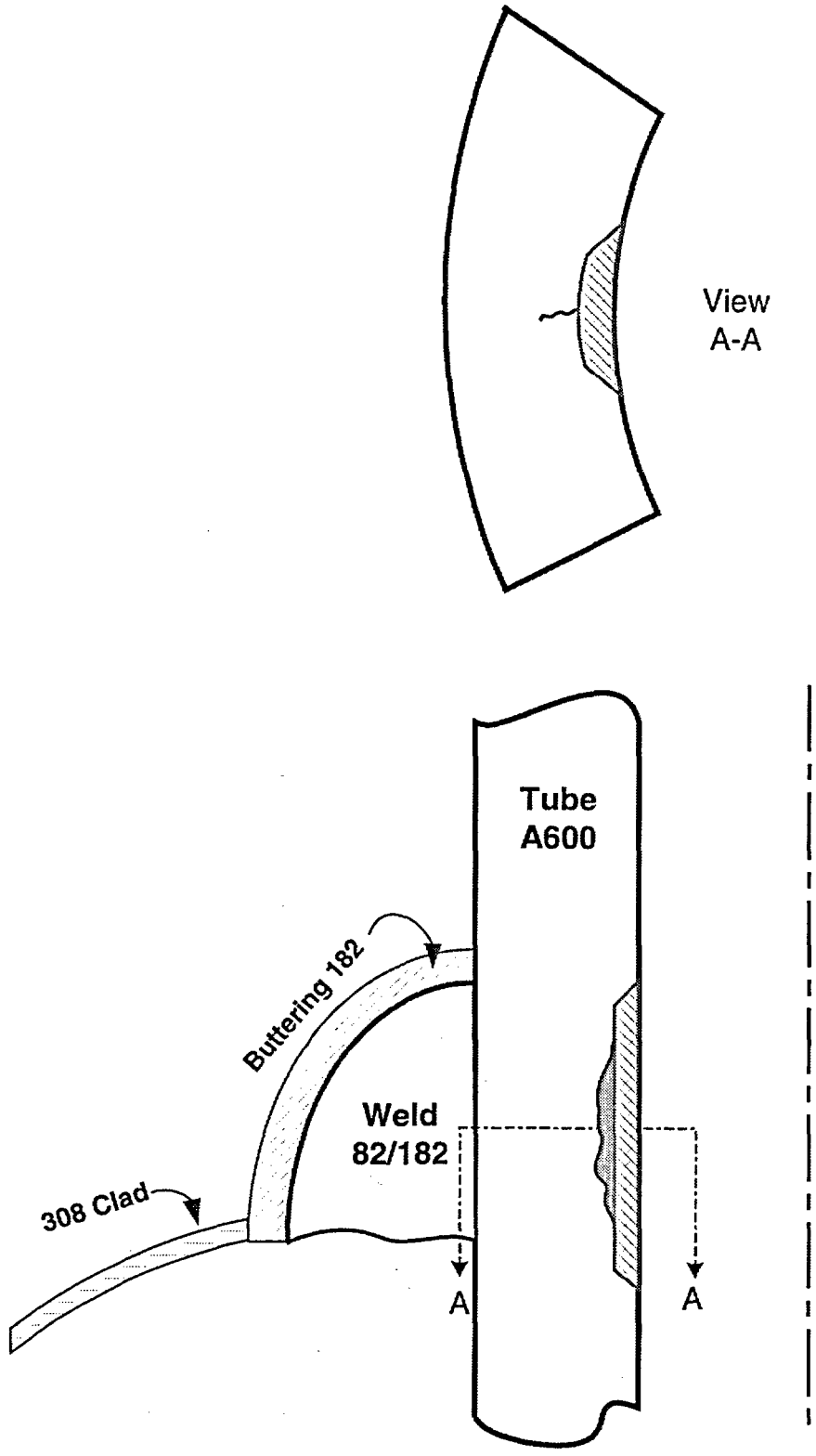

Figure 1-1 Application of the Embedded Flaw Repair to a Flaw in the Head Penetration Tube Inside Surface

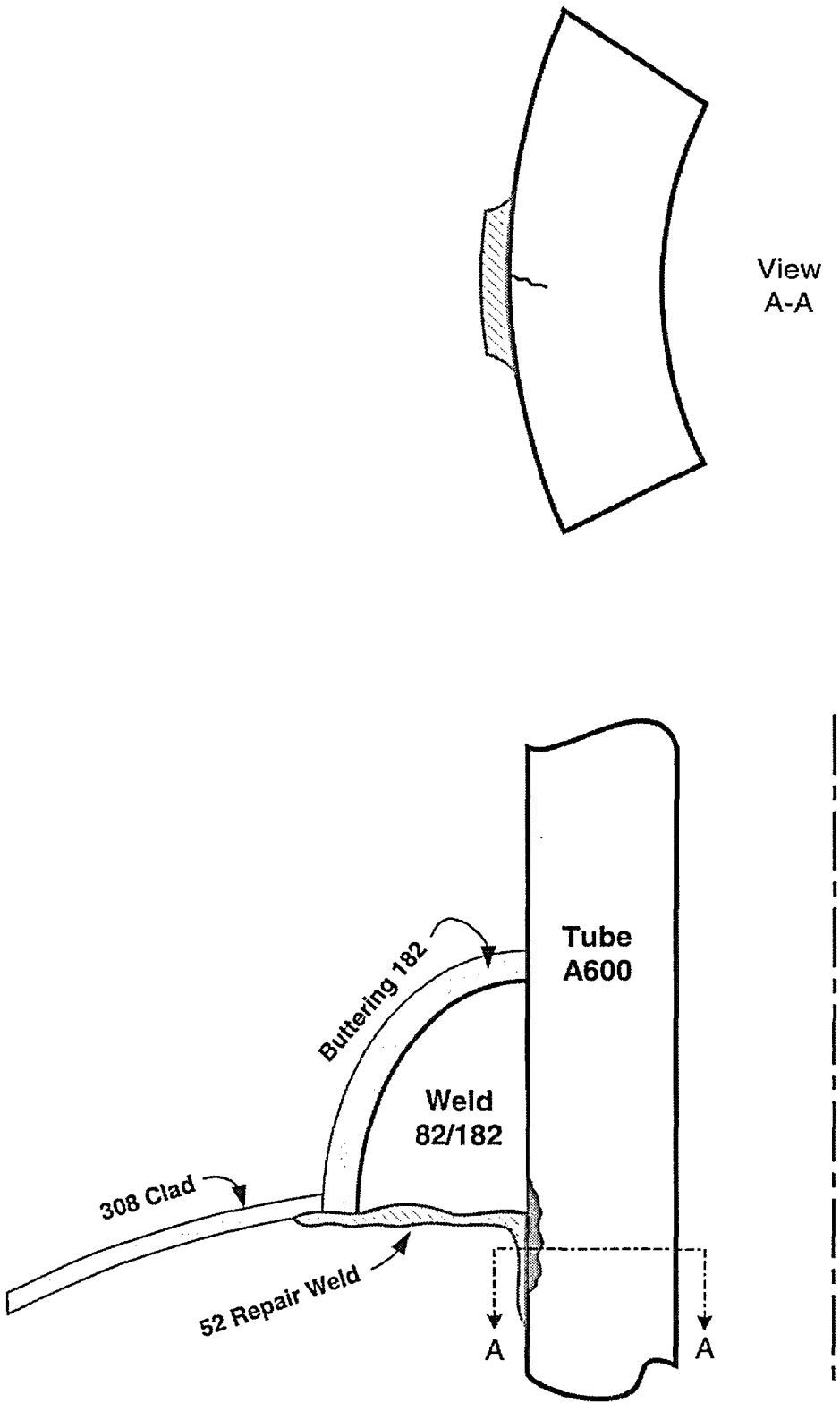

Figure 1-2 Application of the Embedded Flaw Repair to a Flaw in the Head Penetration Tube Outside Surface, or to a Flaw in the Attachment Weld (J-Weld)

2 THE EMBEDDED FLAW REPAIR PROCESS AND ITS IMPLEMENTATION

2.1 PROCESS DESCRIPTION

The Westinghouse approach to address flaws in head penetration tubes and their J-weld attachment welds is the embedded flaw repair process. The embedded flaw repair provides a non-structural barrier to the area of interest in order to stop the corrosion process. Alloy 52 is applied over the cracked Alloy 600 material using multi-pass overlay welding techniques. The welding is accomplished by "machine welding" using remotely operated equipment specifically developed for these applications.

[

]^{a,c,e}

2.2 REPAIR SCENARIOS

Three different crack scenarios can be repaired using the embedded flaw method: Axial or circumferential cracks on the inner surface of the penetration tube, axial cracks in the J-weld and tube to J-weld interface, and axial cracks on the outer surface of the penetration tube below the J-weld. The repair method may also be applicable for a fourth scenario, circumferential cracks in the tube OD, but suitability must be judged on a case-by-case basis.

2.2.1 Axial or Circumferential Cracks in the Penetration Tube Inner Surface

[If an axial or circumferential flaw is found in the penetration inner surface, the thermal sleeve (if present) must be removed to provide access for repair. A band of material over the crack area is excavated utilizing Electrical Discharge Machining (EDM). The resulting groove is inlaid with Alloy 52 weld to embed the flaw. The groove depth is at least 3/16" to allow for three layers of weld material. The welding is done using the GTAW machine process using custom equipment developed specifically for this application. After welding, EDM is again used to restore the penetration tube to its original inside dimension. Finally, an abrasive honing tool may be used to remove the EDM recast layer and smooth the tube surface for the final acceptance NDE.

]^{a,c,e}

Figure 2-1

2.2.2 Axial Crack in the Penetration J-Weld and Tube to J-Weld Interface

[

]^{a,c,e}

[

]^{a,c,e}

The thermal sleeve (if present) must be removed above the J-weld region to allow for repair tooling access. Upon completion of the inspection and/or repair, a replacement lower thermal sleeve will be welded to the thermal sleeve remnant inside the penetration. This will restore the thermal sleeve to its original configuration.

[

]a,c,e

Figure 2-2

2.2.3 Axial Crack on the Penetration Tube OD (Below the J-Weld)

[

]a,c,e

[

]a,c,e

Figure 2-3

2.2.4 Circumferential Crack in the Penetration Tube

[

]a,c,e

2.3 QUALIFICATION OF THE EMBEDDED FLAW REPAIR PROCESS

[

]a,c,e

[

]a,c,e

2.4 NDE REQUIREMENTS

Type of Flaw and Location	Type of NDE Required
Axial Crack in the J-Weld and/or Tube to J-weld Interface	Perform Weld – Perform Final Visual and Surface Exam (Dye Penetrant Test/Eddy Current) Acceptance per ASME Section (NB-4424) (NB-5352) respectively
Axial Crack on Tube ID	Perform Excavation – Perform Penetrant Test Perform Weld – Perform Final Visual and Surface Exam (Dye Penetrant Test/Eddy Current) Acceptance per ASME Section (NB-4424) (NB-5352) respectively
Axial Crack on OD of Tube Below the J-Weld	Perform Weld – Perform Final Visual and Surface Exam (Dye Penetrant Test/Eddy Current) Acceptance per ASME Section (NB-4424) (NB-5352) respectively

2.5 CHEMISTRY OF THE LAST PASS WELD

[

]a,c,e

[

]a,c,e

Table 2-1 Major Element Chemical Composition of Alloy 52 Embedded Flaw Repair									
	Wt %								
Location Description		C	Mn	Ni	Fe	Cr	Al + Ti	Nb	Mo
Bar per SB-166	Min			58.0	7.0	27.0			
	Max	0.05	0.5		11.0	31.0	-	-	-
ERNiCrFe-7 per SFA 5.14	Min			54.5	7.0	28.0			
	Max	0.04	1.0	63.5	11.0	31.5	1.5	0.1	0.5

a,c,e

* not signif - if detected, analysis was not statistically significant

3 BASIS FOR RELIEF

The embedded flaw repair technique is considered a permanent repair that will last through plant life extension because as long as a Primary Water Stress Corrosion Cracking (PWSCC) flaw remains isolated from the primary water (PW) environment it cannot propagate. Since Alloy 52 (690) weldment is considered highly resistant to PWSCC, a new PWSCC crack should not initiate and grow through the Alloy 52 overlay to reconnect the PW environment with the embedded flaw. The resistance of the alloy 690 material has been demonstrated by laboratory testing for which no cracking of the material has been observed in simulated PWR environments, and in approximately 10 years of operational service in steam generator tubes, where likewise no PWSCC has been found. Details of the service experience are given in Section 4 of this report. This experience has been documented in EPRI Report TR-109136, "Crack Growth and Microstructural Characterization of Alloy 600 PWR Vessel Head Penetration Materials," [6] and other papers.

Additional flaw evaluation per IWB 3600 was not considered necessary for an embedded flaw repair. There is no concern for further propagation of the flaw after weld repair because the repair totally seals off the crack from the water environment. Even for a flaw, which extends through the penetration wall thickness, the embedded flaw repair could be applied to both the ID and OD surfaces to ensure the flaw was captured.

The critical flaw length for an axial flaw was discussed and it was stated that the critical size for such a flaw would be through the wall in thickness and over 20 inches in length. The basis for this determination is found on page 12 of WCAP-13565, Rev. 1 [12], where critical length is identified as equal to 13 inches plus the head thickness. The critical length for a circumferential through-wall flaw was shown to be over 90 percent of the circumference. Similar conclusions were reached in the CEOG report CEN-607 [13] for axial flaws, and CEN 614 [14] for circumferential flaws.

Review and approval of these reports by the NRC staff was documented in a November 19, 1993 Safety Evaluation Report [15] transmitted to Mr. W. Rasin, Director of NUMARC at that time. These conclusions remain valid today, despite the passage of almost ten years since they were originally developed. Based upon these approvals, no additional flaw evaluation is needed as part of an embedded flaw repair.

The "embedded flaw" repair methodology has been developed using technology which has been demonstrated in WCAP-13998 [2] entitled "RV Closure Head Penetration Tube ID Weld Overlay Repair." Although this report contains a number of approaches to penetration tube repair, only some of these are used in the embedded flaw repair technique. Some of the key findings of this work are discussed below.

[

]^{a,c,e}

[

]^{a,c,e}

The thermal expansion properties of Alloy 52 weld metal are not specified in the ASME code, as is the case for other weld metals. In this case, the properties of the equivalent base metal (Alloy 690) should be used. For that material, the thermal expansion coefficient at 600°F is 8.2 E-6 in/in/degree F as found in Section II Part D. The Alloy 600 base metal has a coefficient of thermal expansion of 7.8 E-6 in/in/ degree F.

The effect of this small difference in thermal expansion is that the weld metal will contract more than the base metal when it cools, thus producing a compressive stress on the Alloy 600 tube or the attachment weld, where the crack may be located. This effect has already been accounted for in the residual stress measurements reported in the technical basis for the embedded flaw repair [2].

The small residual stress produced by the embedded flaw weld will act constantly, and therefore, should have no impact on the fatigue effects in the CRDM region. Since the stress would be additive to the maximum as well as the minimum stress, the stress range would not change, and the already negligible usage factor, noted above, for the region would not change at all.

4 BACKGROUND AND EXPERIENCE – SCC RESISTANCE OF ALLOY 52

4.1 INTRODUCTION

Alloy 52 is the filler metal used for the joining of Alloy 690 components by either the gas-tungsten arc welding (GTAW) or gas metal arc welding (GMAW) processes. The welding electrode used for the shielded metal arc welding (SMAW) process is Alloy 152. Both of these materials have compositions not differing greatly from the parent Alloy 690 material. Nominal compositions are provided in the following table.

Element	Alloy 690 Base Metal SB-167	Alloy 152 E-NiCrFe-7 SMAW	Alloy 52 ER-NiCrFe-7 GTAW/GMAW
C	0.05 max	0.05 max	0.04 max
Mn	0.5 max	5.00 max	1.00 max
Fe	7 to 11	7 to 12	7 to 11
P	-	0.03 max	0.02 max
S	0.015 max	0.015 max	0.015 max
Si	0.5 max	0.75 max	0.5 max
Cu	0.5 max	-	0.3 max
Ni	58 min	Bal	Bal
Co	-	-	-
Al	-	0.50 max combined	1.10 max Al or 1.50 max combined
Ti	-		
Cr	27 to 31	28.0 to 31.5	28.0 to 31.5
Nb + Ta	-	1 to 2.5	0.10 max
Mo	-	0.50 max	0.50 max
Other elements	-	0.50 max	0.50 max

Essentially coincident with the introduction of Alloy 690 as the material of choice for nuclear applications, Alloys 52 and 152 were introduced for fusion welding applications with 690.

The following paragraphs provide a summary of the experience with respect to these filler metals in service and in laboratory testing. As a point of interest, a summary of the background and corrosion resistance of Alloy 690 is provided in Appendix A. This summary was prepared to endorse the selection of Alloy 690 for SG tubing applications. It will be noted that, in view of the apparent immunity of Alloy 690 to PWSCC, nearly all of the testing reported in the literature cited has been in faulted secondary side chemical environments.

4.2 SERVICE EXPERIENCE

Steam Generators. The majority of the operating plant experience with Alloy 690 and the weld metals Alloys 52 and 152 is associated with replacement steam generator (SG) programs beginning in approximately 1994 with the Delta 75 replacements for V. C. Summer. In addition to the exclusive use of Alloy 690 for the SG heat transfer tubing applications, the weld metals were used for a range of applications in which contact with primary reactor coolant was required. A brief summary of the weld metal applications, primarily for Westinghouse-designed components, follows.

Plant	efpy	Component	Material	Application
New and Replacement Steam Generators				
V. C. Summer	7 +	SG nozzle welds	Alloy 52 and/or Alloy 152	Buttering over Alloy 82/Alloy 182 welds
		Safe end-nozzle welds		
		Divider plate-channel head & stub runner		Final weld layer (in contact with RCS)
N. Anna 1	7 +	Tubesheet cladding	Alloy 52 and/or Alloy 152	All buttering, cladding and welding operations
N. Anna 2	5 +	SG nozzle welds		
Kori 1	5 +	Safe end-nozzle welds		
Shearon Harris	3 +	Divider plate-tubesheet welds		
S. Texas 1	3			
S. Texas 2	1 +			
ANO-2	2			
Farley 1	2			
Farley 2	1 +			
Kewaunee	3			
Sequoyah 1	In mfgrg	Tubesheet cladding	A52/A152	
Ulchin 5 and 6	In mfgrg	Tubesheet cladding, nozzles, partial penetration welds	A52/A152	All buttering, cladding and welding operations
Other Components				
Sequoyah 1; N. Anna		Canopy seal overlays	A52/A152	
Mihama 1		CRDM replacements	A52/A152	Full penetration weld
Calvert Cliffs 1	2000	Quick-Lok repairs	A52/A152	Full penetration weld
Fort Calhoun, Waterford 3	1999, 2000	PZR nozzle repairs	A52/A152	Partial penetration welds
ANO 2; Palo Verde 2	2000	PZR heater sleeve repairs	A52/A152	Partial penetration welds
SONGS 2 & 3	1997-1998	PZR steam space and side shell nozzles; HL and CL A600 nozzle repairs	A52/A152	Partial penetration welds
D. C. Cook 2	~ 5 (1996)	CRDM nozzle repair	A52/A152	Overlay repair

In addition to these Westinghouse units, similar experience has been accrued with replacement SGs in Europe and in Japan, and in B&W replacement units for domestic PWRs.

There have been no reported instances of environmental degradation of any kind for any of these applications; this includes both the Alloy 690 base metal and the Alloy 52 or Alloy 152 weld metals.

This experience is fully consistent with expectations from laboratory testing performed to support the qualification of these materials. This class of austenitic nickel-base alloys, containing greater than 27 wt. pct. chromium, has exhibited full resistance to primary water stress corrosion cracking (PWSCC), to the extent that they are generally regarded as immune to this form of environmental degradation.

This experience, combined with the growing operating plant experience, also provided the basis for the use of Alloys 52 and 152 for the recent primary loop nozzle repairs at V. C. Summer.

Head Penetrations. The best example of service experience of an Alloy 52 weld repair is provided by the experience of the D. C. Cook Unit 2 embedded flaw repair. Penetration number 75 at this plant was found to have an inside surface flaw with a depth of approximately 40 percent of the tube wall thickness. This penetration was repaired with the embedded flaw repair process in 1996, and the repair was re-inspected in January of 2002.

The inspection of January 2002 was carried out with both dye penetrant and eddy current testing. The penetrant examination showed no indications, as did the eddy current testing. The eddy current results are more quantitative, and will be discussed here in some detail. The method was demonstrated and qualified under a program in response to the NRC Generic Letter 97-01. The process uses an eddy current coil with high-resolution gray scale imaging, with a magenta response at 50 percent of the amplitude of the calibration notch (0.004 inch long and 0.040 inch deep). This was shown empirically to correspond to the response to actual PWSCC. An example of such a response is shown in Figure 4-1, which shows actual clustered axial flaws in a penetration tube. The coil design is optimized for high spatial resolution, in order to distinguish individual responses among clusters of cracks, such as those shown in Figure 4-1.

This eddy current testing and display process was applied to the D.C. Cook penetration 75 in January 2002, and the results are shown in Figure 4-2. The results show no evidence of cracking after six years of service.

4.3 LABORATORY EXPERIENCE

For the reasons stated above, i.e., the fact that thorough laboratory testing and field experience to date have indicated no basis for concern over PWSCC with Alloy 690, relatively little testing for either crack initiation or crack propagation has been performed for either the base metal or the weld metals over the last ten or more years. The only research with which Westinghouse is familiar is cited below.

Psaila-Dombrowski et al. [10] evaluated the SCC resistance of Alloy 152 welds in primary water environments using constant extension rate tests (CERT) at 343°C (650°F). Examination of the fracture surfaces indicated no environmentally-related degradation. All fracture occurred by ductile rupture.

Psaila-Dombrowski et al. [11] performed a series of CERT tests on Alloys 52 and 152 weldments in simulated primary water at 343°C (650°F). After testing for periods up to 4122 hours, environmentally-related crack propagation was not observed.

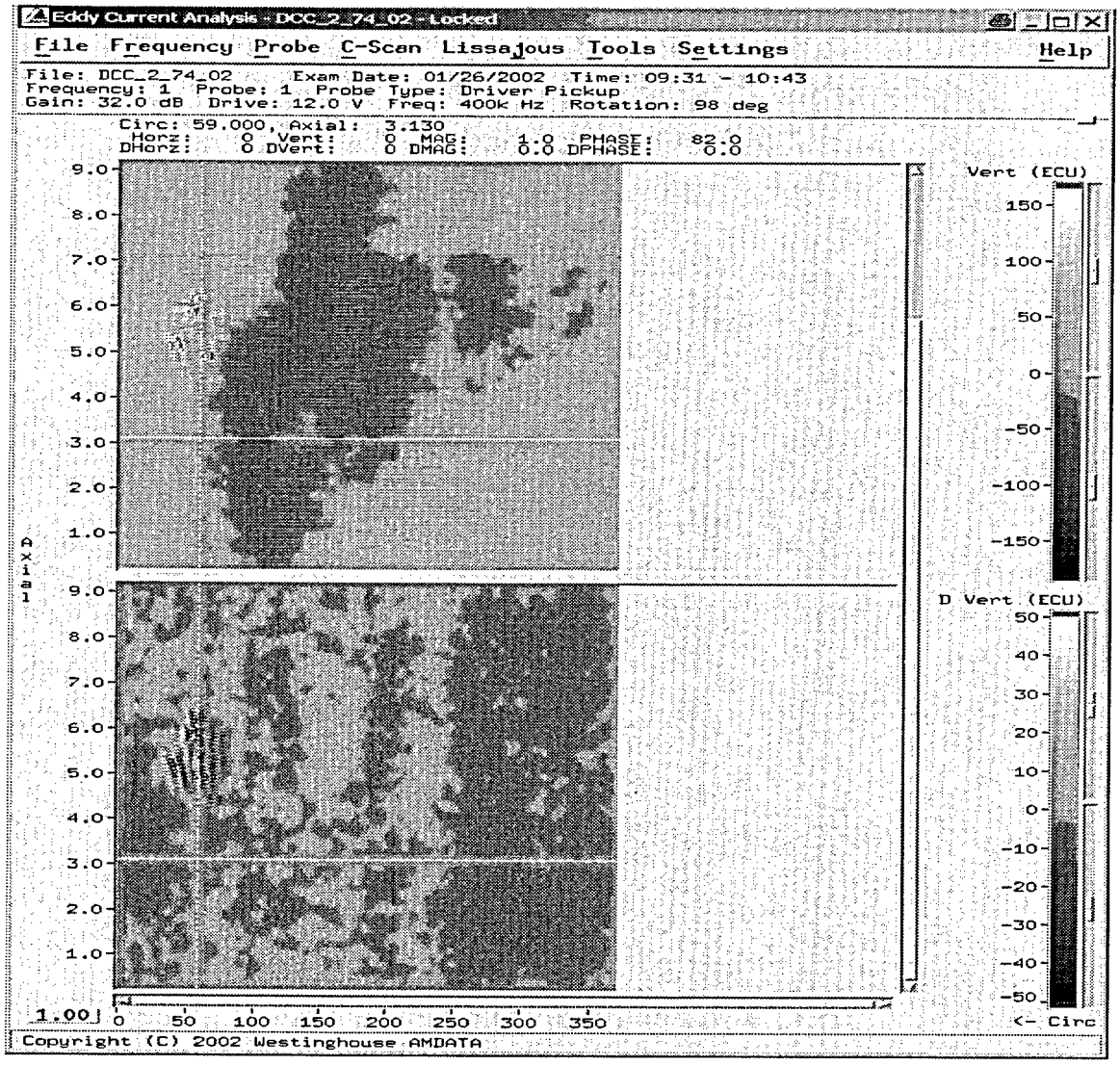

Figure 4-1 ECT View of Craze Cracking

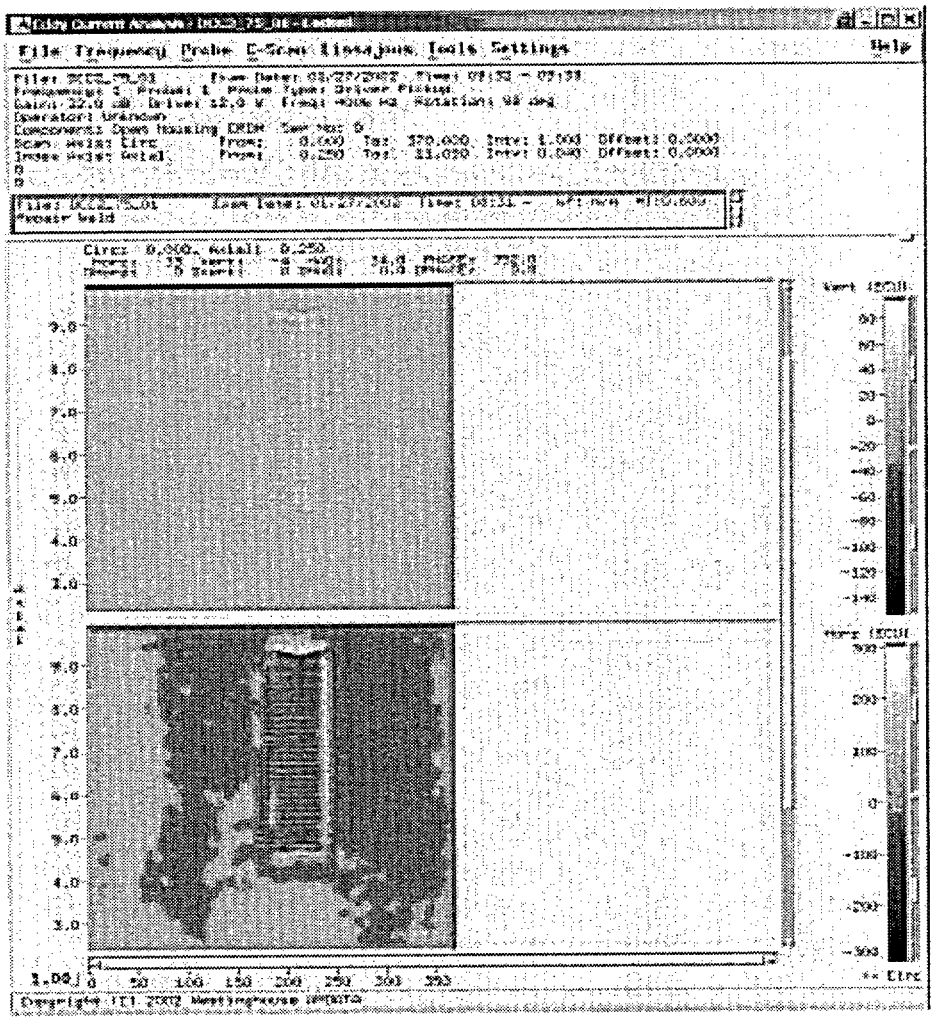

Figure 4-2 ECT View of 1996 Repair, Taken in 2002

5 NDE CAPABILITIES

Westinghouse has participated in several demonstration efforts to determine the effectiveness of their NDE technology to detect and size PWSCC cracking. These demonstration efforts include the EPRI sponsored demonstrations associated with NRC Generic Letter 97-01 and NRC Bulletin 2001-01 as well as Westinghouse internal demonstrations.

Demonstration 1: EPRI Demonstration Pursuant to NRC Generic Letter 97-01

Westinghouse successfully performed procedure demonstrations using the eddy current and ultrasonic examination methods pursuant to NRC Generic Letter 97-01. See Table 5-1 for a detailed summary of Westinghouse Generic Letter 97-01 demonstrations.

The Generic Letter 97-01 demonstrations were designed to quantify a vendor's capability to detect axial and circumferential flaws initiating on the inside diameter of the RPV penetration tubes. Mock-up flaws were implanted in the tubes using the electric discharge machining process, and squeezed to dimensions that simulate PWSCC using cold isostatic processing. The Generic Letter 97-01 demonstrations were conducted and documented by EPRI. These demonstrations were blind; that is, candidates were not given any information about the number, size, or location of flaws.

Details of NDE examination demonstrations pursuant to NRC Generic Letter 97-01 are documented in EPRI Report TR-106260 entitled, "Demonstrations of Inspection Technology for Alloy 600 CRDM Head Penetrations." The abstract of EPRI Report TR-106260 states: "A program has been developed to enable utilities to demonstrate procedures for inspection of alloy 600 control rod drive mechanism penetrations. The program was developed in coordination with utilities and original equipment manufacturers through a Nuclear Utility Management and Resources Committee Ad Hoc Advisory Committee and addresses ultrasonic and eddy current procedures used for detection of primary water stress corrosion cracking initiating on the inside surface of penetrations. Realistic, full-scale mockups were designed and fabricated to incorporate the essential features of installed penetrations such as geometry, clearances, distortion caused by welding, and magnetic deposits and scratches that affect inspection. Intentional flaws were introduced with methods that allowed accurate knowledge of the true flaw size and location. Mockup and flaw fabrication methods were qualified by comparing the ultrasonic and eddy current responses of the mockup flaws with real primary water stress corrosion cracking in penetration samples from Electricite de France's Bugey plant. The comparisons show that the mockup flaws simulated real PWSCC closely in all essential features important to inspection demonstration. A protocol was developed for conducting demonstrations to measure flaw detection efficiency, flaw location and sizing accuracy, resolution of closely spaced flaws, and false call performance.

The Generic Letter 97-01 demonstrations efforts documented by EPRI Report TR-106260 have been reported and observed previously by the NRC. The EPRI report concludes the following: "The results of the qualification activities demonstrated clearly that the procedures applied were highly effective at detecting flaws. Flaw location and sizing accuracy was also measured and shown to be compatible with flaw evaluation criteria developed by the Ad Hoc Advisory Committee."

Demonstration 2: MRP Demonstration Pursuant to NRC Bulletin 2001-01

The MRP developed a demonstration program to detect outside diameter initiated flaws as a result of the Oconee PWSCC flaw findings. See Table 5-1 for a detailed summary of Westinghouse demonstrations for the MRP. The initial MRP demonstrations were attended and reviewed by NRC personnel.

The focus of the demonstration program was the examination for safety-significant cracking on the outside surface of the penetration base material above or near the J-groove weld. Examination of the J-groove weld was not included in the demonstrations.

The demonstration program consisted of two parts:

1. The first part demonstrated the capability to detect real PWSCC using samples removed from Oconee 3 penetrations. The Oconee samples were small segments of RPV penetration nozzles that contained PWSCC. The samples were removed during the repair process at Oconee 3. These samples contain normal and off-axis PWSCC. The off-axis flaws were used to determine the capability to detect circumferential flaws that were oriented at the maximum weld angle (outermost penetration).

2. The second part of the demonstration was on a full-scale mockup consisting of a penetration welded into a simulated section of a RPV head. The mockup contained several simulations of outside diameter flaws. However, other pertinent inspection variables were determined as follows:

   - ability to maintain contact in the presence of surface distortion caused by welding
   - access limitations
   - consistency of scan patterns
   - false call sources
   - accurately locating the position of the weld
   - accurately positioning flaws with respect to the weld

The demonstration on the full-scale mock-up was performed only with a blade probe and not with the open housing scanner. However, a subsequent demonstration using the open housing scanner was used to inspect an Oconee field removed sample (#56C). The axial shooting PCS24 probe was capable of detecting the axially oriented and off angle OD PWSCC in this sample.

Demonstration 3: Westinghouse Demonstration of J-Groove Weld and Penetration Tube Outside Diameter Surface Eddy Current Technique

In order to demonstrate the capability of eddy current for the J-groove welds and penetration tube outside diameter surfaces, Westinghouse conducted a series of laboratory tests consisting of the following:

1. Manufacture and inspection of alloy 182 welded mockups with PWSCC produced in autoclaves.
2. Inspection of a removed nozzle section from Oconee.
3. Inspection of penetrations in an unused reactor pressure vessel head.

The eddy current coil design is an X-point configuration used in the driver pickup mode. A mechanical end effector was built to perform the necessary motions to deliver the eddy current coils to the nozzle and the J-groove weld surface to provide complete inspection coverage of the required region.

A calibration block was fabricated with a series of EDM notches. A series of mockups were made by welding two carbon steel plates together with Alloy 182 weld metal. These plates were then subjected to three point bending and placed in an autoclave to produce PWSCC. Periodically these samples were removed and inspected with dye penetrant testing. When surface flaws reached lengths of 6-9 mm, two samples were removed and used as test pieces.

The eddy current test procedure was used to inspect this sample. Based on the eddy current results, eight individual PWSCC responses were identified and marked for sectioning. Sectioning was performed at the midplane of each of the eight indications and the flaw depths were measured. During the metallographic sectioning, it was noted that the PWSCC was very tight and the finest grit was required in order to outline the cracks which had depths in the range 0.080" to 0.400". Good correlation with actual crack lengths was achieved.

In order to address detection of PWSCC in the nozzle penetration outside diameter surfaces, additional testing was performed on a removed sample from Oconee, sample number 56C. Eddy current results correlated well with the actual sample conditions.

After completing this portion of the mockup testing, an actual RPVH was inspected. An unused four-loop head from a cancelled plant was used to determine scanner coverage and background noise from actual J-groove welds. The background noise from the welds was nominally 0.3 volts, which provided a 10 dB signal to noise ratio for the PWSCC response. In addition, no false positives were reported using the analysis guidelines developed for this inspection. Background noise and geometric indications were distinguished from flaws by signal phase differences.

The combination of laboratory and field testing have demonstrated the following:

1. Eddy current is suitable for the detection of surface and slightly subsurface PWSCC in alloy 182 weld metal and penetration nozzle OD.

2. Eddy current has a sufficient signal to noise ratio for the inspection of J-groove welds.

3. The false positive call rate is very low.

4. The length sizing capability is more than adequate for the intended use.

5. The mechanical scanning equipment is capable of providing proper contact and coverage of J-groove welds and the penetration nozzle OD.

Demonstration 4: EPRI/MRP Demonstration – August/September 2002

The most recent EPRI/MRP demonstration activities were intended to:

- Quantify detection limits of inside-diameter (ID) and outside-diameter (OD) connected flaws from the ID of the penetration tube,
- Document sizing capabilities of ID and OD connected flaws from the ID of the penetration tube,
- Evaluate capabilities to detect defects on the wetted surface of the RVHP attachment weld, and
- Investigate the capability to detect flaws approaching the weld-to-tube interface (triple point flaws) using ultrasonic (UT) inspection from the ID surface of the penetration tube.

Demonstration of WesDyne equipment and procedures was conducted at their Windsor, CT facility during. Open-tube and blade probe UT and ET equipment and procedures were demonstrated. Procedures addressed inspection of the RVHP tube and weld-to-tube interface from the inside surface of the tube.

Results are summarized in the following table:

a,c,e

a,c,e

Table 5-1 EPRI/MRP Demonstration Results

a,c,e

Table 5-1 EPRI/MRP Demonstration Results (cont'd)

WesDyne GrooveMan detection results.

a,c,e

[

]^{a,c,e}

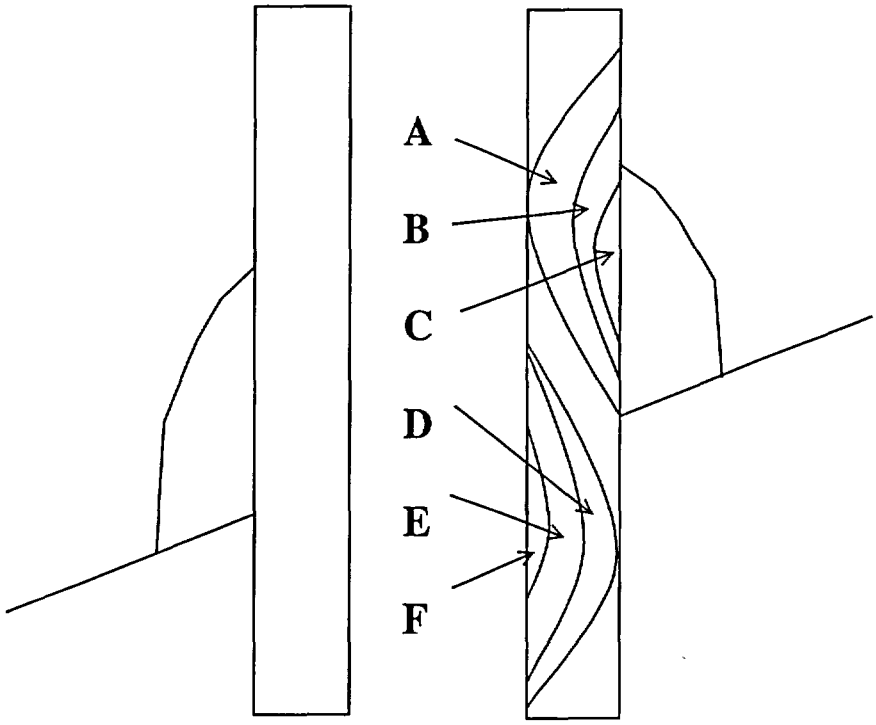

6 SUMMARY AND CONCLUSIONS

The embedded flaw repair technique was developed by Westinghouse in 1994, and involves the deposition of at least three layers of Alloy 52 weld metal to isolate existing flaws and susceptible material from the primary water environment.

The embedded flaw repair technique is considered a permanent repair for a number of reasons. As long as a Primary Water Stress Corrosion Crack (PWSCC) remains isolated from the primary water (PW) environment, it cannot propagate. Since Alloy 52 weldment is resistant to PWSCC, a new PWSCC crack will not initiate and grow through the Alloy 52 overlay to permit the PW environment to contact the susceptible material. The resistance of Alloy 690 and its associated welds, Alloys 52 and 152, has been demonstrated by laboratory testing in which no cracking has been observed in simulated PWR environments, and by approximately 10 years of operational service in steam generator tubes, where no PWSCC has occurred. The crack growth resistance of this material has been documented in EPRI Report TR-109136, "Crack Growth and Microstructural Characterization of Alloy 600 PWR Vessel Head Penetration Materials," [1] and other papers. The service experience has been discussed in Section 4.

The residual stresses produced by the embedded flaw technique have been measured and found to be relatively low [2] because of the small thickness of the weld. This implies that no new cracks will initiate and grow in the area adjacent to the repair weld. There are no other known mechanisms for significant crack propagation in this region because the cyclic fatigue loading is considered negligible. Cumulative Usage Factor (CUF) in the upper head region was calculated to be typically less than 0.2 [3] in the reactor vessel design report, as well as in various aging management review reports.

The thermal expansion properties of Alloy 52 weld metal are not specified in the ASME code, as is the case for other weld metals. In this case, the properties of the equivalent base metal (Alloy 690) should be used. For that material, the thermal expansion coefficient at 600°F is 8.2 E-6 in/in/degree F as found in Section II Part D. The Alloy 600 base metal has a coefficient of thermal expansion of 7.8 E-6 in/in/degree F, a difference of about 5 percent.

This report has presented a description of the process as well as the controls imposed to ensure a good weld. The excellent experience with this repair over six years at D.C. Cook Unit 2 has been described, as well as the lessons learned from the more recent J-weld repair at North Anna Unit 2.

The Westinghouse NDE capabilities have been demonstrated in multiple venues, and the results were summarized in Section 5. This capability is important to ensure that no flaws remain undetected when a repair is implemented.

7 REFERENCES

1. TR-109136, "Crack Growth and Microstructural Characterization of Alloy 600 PWR Vessel Head Penetration Materials," EPRI, December 1997.

2. WCAP-13998, "RV Closure Head Penetration Tube ID Weld Overlay Repair," March 1994. (Westinghouse Proprietary).

3. WCAP-15269, Rev. 1, "Aging Management Review and Time Limited Aging Analysis for the North Anna Units 1 and 2 Reactor Pressure Vessels," September 2001.

4. Rotterdam Welding Procedure 34.08, "Procedure for a combination of manual gas tungsten arc welding and manual gas metal arc welding of solid Inconel (P-Number 43) to solid Inconel (P-Number 43) or to Inconel weld overlay cladding."

5. Rotterdam Welding Procedure 37.02, "Procedure for manual shielded metal arc overlay cladding with Inconel (P-Number 43) of low alloy steel (P-Number 12B)."

6. Rotterdam Drawing 30660-1088, "Top Head Cap."

7. Rotterdam Drawing 30660-1097, "Top Head Cap (Pre Machined)"

8. Rotterdam Drawing 30660-1103, Sheet 1, "Closure Head Assembly C.R.D. Housing Assy."

9. Rao, G.V. and Bennetch, J., "Metallurgical Investigation of Cracking of the Alloy 82/182 J-Groove Weld of the Reactor Vessel Head Penetration Joint at North Anna Unit 2 Station," Westinghouse Report WCAP 15777, January 2002.

10. M. J. Psaila-Dombrowski et al., "Evaluation of Weld Metal 82 and Weld Metal 182 Stress Corrosion Cracking Susceptibility," *Proceedings, Seventh International Symposium on Environmental Degradation of Materials in Nuclear Power Systems – Water Reactors*, NACE Int'l., (1995) 81-91.

11. M. J. Psaila-Dombrowski et al., "Evaluation of Weld Metals 82, 152, 52 and Alloy 690 Stress Corrosion Cracking and Corrosion Fatigue Susceptibility," *Proceedings, Eighth International Symposium on Environmental Degradation of Materials in Nuclear Power Systems – Water Reactors*, ANS (1997) 412-421.

12. WCAP-13565, Revision 1, "Alloy 600 Reactor Vessel Head Adapter Head Cracking Safety Evaluation."

13. Combustion Engineering report CEN-607, "Safety Evaluation of the Potential for and Consequences of Reactor Vessel Head Penetration Alloy 600 ID Initiated Nozzle Cracking," May 1993.

14. Combustion Engineering report CEN-614, "Safety Evaluation of the Potential for and consequences of Reactor Vessel Head Penetration Alloy 600 OD Initiated Nozzle Cracking, December 1993.

15. NRC SER for WCAP-14024 and WCAP-13565 NRC letter from W. T. Russell to W. Raisin, NUMARC, dated November 19, 1993.

16. Abbott, S.L., et al, "Aging Management Review and Time Limited Aging analysis for the North Anna Units 1 and 2 Reactor Pressure Vessels", Westinghouse Electric Report WCAP 15269, June 1999.

APPENDIX A
BASIS FOR SELECTION OF ALLOY 690 FOR STEAM GENERATOR HEAT TRANSFER TUBING

R. E. Gold and D. L. Harrod

A.1 INTRODUCTION AND SURVEY OF CORROSION RESISTANCE

The primary basis for the selection of a steam generator heat transfer tubing material is corrosion resistance. The corrosion behavior of thermally treated Alloy 690TT in relevant steam generator environments, its performance relative to other prominent candidate tubing materials, namely Alloy 600, Alloy 800, and austenitic stainless steels, and a brief survey of recent corrosion research programs with this alloy, are reviewed in the following section. Following the summary and conclusions in the subsequent section, a selected list of references is given, and is complemented more completely in an attached Bibliography.

Corrosion Resistance of Alloy 690

Alloy 690 was adopted as the preferred alloy for steam generator heat transfer application in about 1986 after more than a decade of evaluation and testing. The first application of this alloy was in the replacement Series 54F steam generators at D.C. Cook Unit 2 in May 1989.

The basic corrosion resistance of Alloy 690 (Alloy 690TT) to primary side or "normal" faulted secondary side environments had been fairly well established prior to its adoption. This research included the use of high temperature primary water and accelerated primary side environments such as 400°C doped steam to determine the primary side resistance, and testing in caustic, caustic-plus sulfate, caustic-plus CuO, and acid chloride environments for the secondary side. It was largely on the basis of the results of these tests that Alloy 690 was selected to replace mill annealed or thermally treated Alloy 600. At the present time, Alloy 690TT is the material of choice for all new and replacement steam generators built by Westinghouse, Framatome, Babcock & Wilcox International (BWI), and Mitsubishi Heavy Industries (MHI). Only Siemens is using an alternate material, Alloy 800 Mod.

Since the adoption of Alloy 690, laboratory-based research programs have continued on a modest basis. The primary intent of these efforts has been to determine whether or not a previously unidentified "Achilles Heel" exists for this material, or whether specific aspects of tube manufacturing might be modified to further optimize its corrosion resistance.

A brief survey of selected publications relevant to these efforts is provided in the following paragraphs. This survey is intended to be representative, rather than an exhaustive review of the available literature. A bibliography of Alloy 690 publications in the proceedings of International (refereed) Symposia in the period since approximately 1990 is appended to this report.

Recent Corrosion Testing of Alloy 690

In all corrosion tests used to simulate primary side environments Alloy 690TT continues to exhibit total immunity to primary water stress corrosion cracking (PWSCC). Hence, testing of this nature has essentially been abandoned.

Intergranular carbide precipitation has been demonstrated to enhance the stress corrosion cracking (SCC) resistance of nickel-chromium-iron alloys in nuclear steam generator environments. For Alloy 690TT, as was the case for Alloy 600TT, the intergranular carbide precipitation is achieved by a final thermal treatment at ~720°C for times from 5 to 15 hours. While the precipitation reaction occurs in fairly short times at this temperature, the extended time permits the replenishment of chromium to the region adjacent to the grain boundaries, thereby avoiding "sensitization."

That Alloy 690 contains 30% chromium, and therefore is much less susceptible to grain boundary chromium depletion than lower chromium compositions, offers the possibility that shorter-time higher-temperature thermal exposures may achieve the desired intergranular precipitation more efficiently than the ~720°C/5-15 hour procedure. EPRI sponsored a research program in which caustic tests were performed on C-ring specimens of Alloy 690 tubing for which the thermal treatment was effected by 10-minute exposures at 871 or 927°C (Ref. 1). Alloy 690 specimens given standard thermal treatments were included for comparison. For the period of exposure, involving times up to 9000 hours, essentially no difference could be seen for tubing prepared using the various thermal treatments. However, in view of the perceived greater control afforded by the use of batch-loaded vacuum furnaces compared to continuous inert gas belt furnaces, none of the commercial tube manufacturers has continued with further evaluations of the higher-temperature, shorter-time thermal treatment process.

CIEMAT, the Spanish utilities' laboratory, has conducted tests comparing the stress corrosion cracking resistance of Alloy 600MA, Alloy 690TT, and Alloy 800 exposed at 350°C to the following environments (Refs. 2, 3):

Caustic Environments

- 10% NaOH
- 10% NaOH + 0.1M PbO (2% PbO)
- 10% NaOH + 0.01M PbO (0.2% PbO)
- 4% NaOH + 0.002M PbO (0.04% PbO)
- 10% NaOH + 0.01% CuO
- 50% NaOH + 5% $Na_2S_2O_3$ (sodium thiosulfate)

Acidic Environments

- 0.75M Na_2SO_4 + 0.25M $FeSO_4$
- 0.75M Na_2SO_4 + 0.25M $FeSO_4$ + 0.1M PbO (2% PbO)
- 0.4M $NaHSO_4$ + 0.2M $FeSO_4$ + 0.2M Na_2SO_4
- 50 ppm NaCl + 50 ppm $CuCl_2$

The 1000-hour exposures of the 2% strained C-rings showed clear superiority of Alloy 690TT over both Alloy 800 and Alloy 600MA in pure and CuO-doped NaOH. Alloy 690TT exhibited degradation only in

the 10% NaOH environments which contained PbO, and in the 50% NaOH + 5% sodium thiosulfate environment.

None of the acidic environments caused any degradation of Alloy 690TT, whereas they caused IGSCC of both Alloy 800 and Alloy 600MA. In all test environments, even those that caused some degradation, Alloy 690TT exhibited greater resistance to SCC than either Alloy 600MA or Alloy 800.

Vaillant et al. (Ref. 4) performed a series of 350°C corrosion tests to evaluate the relative role of mill annealing temperature, extent of grain boundary precipitation, and carbon content on the resistance of Alloy 690TT to SCC in NaOH solutions. NaOH concentrations of 4%, 10%, and 50% were used in pressurized capsule tests with applied stresses up to 90% of the 350°C yield strength. A range of Alloy 690 tubing products was tested, including materials that would not meet the current product specification with regard to grain size or grain boundary carbide density. After exposures up to 14,000 hours, the authors reported that Alloy 690 prepared with high final mill annealing temperature (> 1040°C and preferably > 1070°C), carbon content in the range 0.015 - 0.021%, and thermally treated to produce a high density of grain boundary carbides, exhibited optimum resistance to caustic SCC. The manufacturing specifications for Alloy 690TT meet these requirements.

Doherty et al. (Ref. 5) used 316°C constant extension rate tests (CERTs) in 10% NaOH to study the influence of minor microstructural differences on the corrosion resistance of Alloy 690TT. The test program was designed to include Alloy 690TT prepared by several different vendors and reflected variations in both the melting practice - e.g., air induction, argon-oxygen decarburization (AOD), vacuum-oxygen decarburization (VOD), or electroslag remelting (ESR) - and final tube reduction practice (pilgering or drawing).

The results of this test program were interpreted as confirming the importance of a high density of grain boundary carbides in enhancing the resistance to caustic SCC. No significant correlations could be drawn between the CERT results and tubing chemistry, level of intragranular carbides, inclusion content, melt practice, and mill anneal/thermal treatment practices. The authors suggest that the tube making process may be important but, conversely, state that the effect of tube making can not be demonstrated from their results since ..."The resultant microstructure for drawn tubing cannot be distinguished from that in pilgered tubing."

Sarver et al. (Ref. 6) also published the results of 316°C CERT tests in 10% NaOH of a variety of Alloy 690TT materials. Again, as in the previous discussion, the authors note the apparent importance of grain boundary carbide coverage in establishing caustic SCC resistance (but unfortunately do not provide microstructures to support this observation). They further conclude that no clear correlations were observed between chemistry or thermal processing and microstructure.

Sarver et al. (Ref. 7) have published additional research intended to identify the potential role of variations in manufacturing processes on microstructure and SCC resistance of Alloy 690TT. This research again used CERT tests in 10% NaOH at 316°C. The authors attempted to correlate small variations observed in the SCC resistance of Alloy 690TT produced by a variety of processes in terms of "grain boundary character distributions." They use, in this sense, the classification method devised originally by Watanabe (Ref. 8), whereby grain boundaries characterized by certain special or low angle crystallographic relationships (coincidence site lattice model) are expected to display special or improved

properties. Simply stated, the greater the density of these special, low energy, boundaries, the greater the resistance to SCC. The authors suggest that the relative ease with which these special boundaries apparently form in Alloy 690TT may have a significant role in its enhanced corrosion resistance. However, nothing presented, or referred to in the discussion which followed this presentation, identified how manufacturing processes may contribute to variations in this condition.

Several papers have been published recently documenting the results of corrosion tests of Alloy 690TT in caustic-plus-lead environments. This is, in fact, one of the few environments that can induce significant degradation in this alloy. McIlree (Ref. 9) and Sarver et al. (Ref. 10) reported the results of exposures of nine heats of Alloy 690 C-rings to a 4% NaOH-plus 125 ppm PbO environment at 324°C. The objective of these tests was to determine the influence of variations in the final mill annealing temperature and the thermal treatment time and temperature on the resistance to Pb-induced SCC.

Alloy 690 not given a thermal treatment cracked in times on the order of 1000 hours, with the lower temperature mill anneals being least resistant. The materials which exhibited the greatest resistance to SCC in 7000 hour exposures were those given relatively high temperature final mill anneals (> 1070°C). Little variation was seen over the range of thermal treatments. This latter observation is not particularly surprising since Pb-caustic SCC occurs in Alloy 690 by transgranular rather than intergranular cracking. The presence or lack of carbide precipitation at the grain boundaries would, therefore, be expected to play a relatively minor role.

The authors concluded that no clear correlations were observable between the resistance of Alloy 690 to Pb-caustic SCC and processing parameters (melting process, hot/cold working processes, final annealing temperature or thermal treatment practice). Neither were there any correlations between Pb-caustic SCC and material property parameters (chemistry, mechanical properties, grain size, inclusion rating, and carbide content and distribution). The Pb-caustic SCC appeared to be related solely to environmental test parameters, becoming more severe with increasing time, temperature, Pb concentration and stress. The Alloy 690TT tubing procured from Sandvik exhibited the best performance of all materials tested.

Included in the bibliography are a number of references which report the results of Pb-caustic SCC tests of Alloy 690TT. There is little question about the aggressiveness of this environment toward Alloy 690 - and Alloys 600 and 800 as well. The strategy that must be adopted by the utility is to take all possible measures to ensure minimal transport of lead into the secondary side SG water. Note that, with the exception of two instances – one in Canada and one in Europe - where Pb shielding blankets were inadvertently left inside SGs after maintenance operations, Pb-induced SCC has been a rarely observed form of degradation in SGs operating with Alloy 600 tubing.

Pierson et al. (Ref. 11, 12) have reported the results of a series of tests of Alloys 600, 690, and 800 in acidic environments at 320°C. The specimens were prepared as freestanding roll-expanded tube sections contained within capsules that contained the test environment. The cover gas was varied to include pure argon and argon containing 5% hydrogen. In the first phase of these experiments, acidic environments consisting of mixtures of Na_2SiO_3, Fe_3O_4 or $FeSO_4$, and cationic resins with and without dilute additions of PbO were found to very seriously degrade Alloy 600 and, to a lesser extent attack Alloy 800, in exposures ranging from 220 to greater than 2000 hours. For periods up to nearly 2000 hours, Alloy 690TT was fully immune to attack.

In a subsequent phase of this program, additions of approximately 0.1m concentrations of CuO and Cu_2O to these acidic environments induced significant cracking of Alloy 690TT when the cover gas was pure argon. When the cover gas contained 5% hydrogen, the Alloy 690TT did not crack. The testing was extended to determine if a dilute concentration of hydrazine (1 ppm), used to condition secondary water in many PWRs, would similarly inhibit degradation in the presence of copper oxides. Hydrazine was successful in this regard. The authors speculate that this inhibition effect may be due to a direct reduction of the copper oxides by the hydrogen or hydrazine. Several reviewers have acknowledged the results as reliable but have questioned the representativeness of the test conditions (artificial geometry, extremely high applied stresses, and a highly fictitious sludge composition). These reservations notwithstanding, these experiments enforce the position that during periods of wet layup and secondary side maintenance, it is prudent to maintain an active partial pressure of hydrogen or hydrazine, or as a minimum to ensure the exclusion of oxygen.

A.2 SUMMARY AND CONCLUSIONS – ALLOY 690TT CORROSION RESISTANCE

Alloy 690TT was chosen for SG heat transfer tubing applications on the basis of its superior corrosion resistance. This was true in the mid-1980s and remains true today. None of the recent corrosion test results suggest any basis for changing or revisiting this decision. In virtually every head-to-head comparison of Alloy 690TT with Alloy 800 Mod, Alloy 690TT continues to demonstrate superior performance.

Several years ago, Westinghouse collaborated with the Electric Power Research Institute in developing a summary comparison of the relative corrosion resistance of Alloy 600MA, Alloy 600TT, Alloy 690TT, Alloy 800 Mod, and austenitic stainless steels in a broad range of corrosive environments. Only in the area of Pb-caustic corrosion does Alloy 690TT fare poorly, as discussed above; this is true, however, of the other alloys as well, although Alloy 600 performs slightly better than the other candidates.

Although this ranking was developed five or six years ago, a close review indicates that no data of which Westinghouse is aware would alter the rankings indicated. The ranking of Alloy 690TT is particularly impressive when the excellent field performance of Alloy 800 Mod is acknowledged. This latter alloy, which clearly offers lower resistance to attack in both acid chloride and caustic environments than Alloy 690TT, has established an impressive performance history in German PWRs over the last twenty or so years. It seems reasonable to expect Alloy 690TT to perform even better.

A.3 SUMMARY AND CONCLUSIONS

Alloy 690 was selected as the heat transfer tubing material for replacement steam generators. The primary basis for this selection is the demonstrated superior corrosion resistance of Alloy 690TT to other candidate tubing materials (Alloy 600 and Alloy 800) in all relevant primary side and secondary side steam generator environments. A brief update on the status of recent additions to the corrosion data base for Alloy 690TT was also presented herein. Alloy 690TT fully satisfies all other specification requirements for SG heat transfer tubing. Since the initial selection of Alloy 690 in the mid-1980s, all additional data and information acquired to date further endorses that selection.

A.4 REFERENCES

1. EPRI NP-6703-M, "Effect of Different Thermal Treatments on the Corrosion Resistance of Alloy 690 Tubing," Final Report on Project S408-2, March 1990.

2. CIEMAT (Spain), Untitled presentation on the Comparative Performance of Alloys 600, 690 and 800 in Caustic, and Caustic-plus-other Contaminant Environments, EPRI IGA/SCC Workshop, Airlie, VA, May 1991.

3. M. L. Castano-Marin et al., "Steam Generator Replacement: Inconel 690 TT and Incoloy 800 Mod. as an Alternative to Inconel 600," presented at the European Corrosion Conference Meeting, Barcelona, Spain, July 1993.

4. F. Vaillant et al., "IGSCC Resistance of Alloy 690 in Caustic Solutions," presented at EPRI Steam Generator IGA/SCC Workshop, Minneapolis, MN, October 14-15, 1993.

5. P. E. Doherty et al., "Stress Corrosion Cracking (SCC) Behavior vs. Microstructure for Alloy 690 Steam Generator Tubing," Second International Steam Generator & Heat Exchanger Conference, Toronto, Canada, June 13-15, 1994.

6. J. M. Sarver et al., "Constant Extension Rate (CERT) Testing of Alloy 690 and Alloy 800 Nuclear Steam Generator Tubing," International Symposium - Fontevraud III, Fontevraud, France, September 12-16, 1994, pp. 529-536.

7. J. M. Sarver et al., "The Influence of Manufacturing Processes on the Microstructure, Grain Boundary Characteristics and SCC Behavior of Alloy 690 Steam Generator Tubing," Proc. Seventh International Symposium on Environmental Degradation of Materials in Nuclear Power Systems - Water Reactors, Breckenridge, CO, Aug. 7-10, 1995. Published by NACE; pp. 465-476.

8. T. Watanabe, J. Physics, 46, C4-555 (1985).

9. A. R. McIlree, "Influence of Heat Treatment on the SCC Behavior of Alloy 690 in a Pb-Contaminated Solution," presented at EPRI Technical Advisory Group Meeting, Charlotte, NC, February 7-9, 1996.

10. J. M. Sarver et al., "A Parametric Study of the Lead-Induced SCC of Alloy 690," Proc. Eighth International Symposium on Environmental Degradation of Materials in Nuclear Power Systems - Water Reactors, Amelia Island, FL, Aug. 10-14, 1997. Published by ANS; pp. 208-215.

11. E. Pierson et al., "Resistance en milieu acide des materiaux alternatifs pour tubes de GV (Alliages 690 et 800)," International Symposium - Fontevraud III, Fontevraud, France, September 12-16, 1994, pp. 556-564.

12. E. Pierson et al., "Stress Corrosion Cracking of Alloys 690, 800 and 600 in Acid Environments Containing Copper Oxides," presented at CORROSION 96, paper 96119, NACE International.

13. EPRI NP-6996-SD, "Alloy 690 for Steam Generator Tubing Applications," Final Report on Project S408-6, October 1990.

A.5 BIBLIOGRAPHY ALLOY 690 LITERATURE - INTERNATIONAL FORUMS (SINCE CA. 1990)

FONTEVRAUD INTERNATIONAL SYMPOSIA

Fontevraud I – 2–6 September 1985 (First in Series)

- C. Gimond et al., "Choix de l'alliage 690 pour les tubes de Generateur de Vapeur," pp. 270–279.
- T. Yonezawa et al., "Effect of Heat Treatment on Corrosion Resistance of Alloy 690," pp. 289–296.

Fontevraud II – 10–14 September 1990 (Second in Series)

- G. P. Airey et al., "Inconel 690 Steam Generator Tubing: Material Specification and Corrosion Resistance," pp. 408–417.

Fontevraud III – 12–16 September 1994 (Third in Series)

- N. Hakiki et al., "Etude des films d'oxyde formes sue les alliages a base de nickel 600 et 690 et l'acier inoxydable 316L en milieu primaire," pp. 327–336.
- M. A. Kreider et al., "Corrosion Mode Diagrams for Alloy 690 TT and Alloy 800," pp. 521–528.
- J. M. Sarver et al., "Constant Extension Rate (CERT) Testing of Alloys 690 and 800 Nuclear Steam Generator Tubing," pp. 529–536.
- A. Rocher et al., "Effect of Lead on the OD Degradation of Steam Generator Tubes," pp. 537–547.
- E. Pierson et al., "Resistance in milieu acide des materiaux alternatifs pour tubes de GV (Alliages 690 et 800)," pp. 556–564.
- M. Garcia et al., "Effect of Lead on Inconel 690 and Incoloy 800 Oxide Layers," pp. 571–578.

Fontevraud IV – 14–18 September 1998 (Fourth in Series)

- R. Staehle and Z. Fang, "SCC of Inconel 600 and Inconel 690 in the Mid-Range of pH," pp. 369–380.
- P. E. Doherty, et al., "The Corrosion Performance of Alloy 690 Steam Generator Tubing - An Overview," an attachment to published proceedings.
- T. Larsson and J.-O. Nilsson, "The Influence of Manufacturing Process on Texture and Grain Boundary Distribution in Alloy 690," pp. 595–604.
- P. R. Aaltonen, et al., "The Effect of Environment on the Electric and Electrochemical Properties of Surface Films on Alloy 600 and Alloy 690 in Pressurised Water Reactor Primary Water," pp. 861–872.

INTERNATIONAL SYMPOSIA ON ENVIRONMENTAL DEGRADATION OF MATERIALS IN NUCLEAR POWER SYSTEMS - WATER REACTORS

Fourth International Symposium. Published by NACE. August 6-10, 1989; Jekyll Island, FL.

- D. B. Lowenstein et al., "Etching Techniques and Carbon Analysis for Alloy 690," pp. 5-1 – 5-15.
- J. R. Crum et al., "Contribution to Optimized Specifications for Procurement of Inconel Alloy 690 PWR Steam Generator Tubing," pp. 5-16 - 5-32.
- A. Smith and R. Stratton, "Relationship Between Composition, Microstructure and Corrosion Behaviour of Alloy 690 Steam Generator Tubing for PWR Systems," pp. 5-33 – 5-46.
- J. M. Sarver et al., "The Effect of Thermal Treatment on the Microstructure and SCC Behavior of Alloy 690," pp. 5-47 – 5-63.
- T. M. Angeliu and G. S. Was, "Grain Boundary Chemistry and Precipitation in Controlled Purity Alloy 690," pp. 5-64 – 5-78.
- P. Combrade et al., "Effect of Sulfur on the Protective Layers on Alloys 600 and 690," pp. 5-79 – 5-95.
- K. Yamanaka et al., "Straining Electrode Behavior and Corrosion Film of Nickel Base Alloys in High Temperature Caustic Solution," pp. 5-96 – 5-106.
- J. M. Sarver et al., "Qualification of Kinetically Welded Alloy 690 Sleeves," pp. 5-107 – 5-127.

Fifth International Symposium. Published by ANS. August 25–29, 1991; Monterey, CA.

- K. Norring et al., "Grain Boundary Microstructure, Chemistry, and IGSCC in Alloy 600 and Alloy 690," pp. 482–487.
- D. L. Harrod et al., "The Temperature Dependence of the Tensile Properties of Thermally Treated Alloy 690 Tubing," pp. 849–854.
- A. J. Smith and R. P. Stratton, "Thermal Treatment, Grain Boundary Composition and Intergranular Attack Resistance of Alloy 690," pp. 855–859.
- S. Suzuki et al., "IGA Resistance of TT Alloy 690 and Concentration Behavior of Broached Egg Crate Tube Support Configuration," pp. 861–868.
- Sixth International Symposium. Published by TMS. August 1-5, 1993; San Diego, CA.
- A. J. Smith et al., "The Effect of the Weld Thermal Cycle on the Microstructure and Corrosion Resistance of Alloys 690, 600 and 800," pp. 97–104.
- S. B. Justus and J. J. Eckenrod, "P/M Alloy N690 as a Solution for Intergranular Stress Corrosion Cracking," pp. 113–120.
- M. Helie, "Lead Assisted Stress Corrosion Cracking of Alloys 600, 690 and 800," pp. 179–188.
- W. H. Cullen et al., "Corrosion of Alloys 600 & 690 in Acidified Sulfate and Chloride Solution," pp. 197–206.

Seventh International Symposium. Published by NACE. August 7–10, 1995; Breckenridge, CO.

- D. Costa et al., "Interaction of Lead with Nickel-Base Alloys 600 and 690," pp. 199–208.
- F. Vaillant et al., "Comparative Behavior of Alloys 600, 690 and 800 in Caustic Environments," pp. 219–232.
- K. K. Chung et al., "Lead Induced Stress Corrosion Cracking of Alloy 690 in High Temperature Water," pp. 233–246.
- J. M. Sarver et al., "The Influence of Manufacturing Processes on the Microstructure, Grain Boundary Characteristics and SCC Behavior of Alloy 690 Steam Generator Tubing," pp. 465–476.
- D. A. Mertz et al., "Role of Microstructure in Caustic Stress Corrosion Cracking of Alloy 690," pp. 477–494.
- K. Liu et al., "Effect of Sulfur and Magnesium on Hot Ductility and Pitting Corrosion for Inconel 690 Alloy," pp. 509–518.

Eighth International Symposium. Published by ANS. August 10–14, 1997; Amelia Island, FL.

- J. R. Crum and T. Nagashima, "Review of Alloy 690 Steam Generator Studies," pp. 127–137.
- J. Frodigh, "Some Factors Affecting the Appearance of the Microstructure in Alloy 690," pp. 138–148.
- H. Kajimura et al., "Corrosion Resistance of TT Alloy 690 Manufactured by Various Melting Practices in High Temperature NaOH Solution," pp. 149–156.
- P. E. Doherty et al., "Mechanical-Electrochemical Performance of Alloy 690 Steam Generator Tubing," pp. 157–166.
- S. S. Hwang et al., "Stress Corrosion Cracking Aspects of Nuclear Steam Generator Tubing Materials in the Water Containing Lead at High Temperature," pp. 200–207.
- J. M. Sarver et al., "A Parametric Study of the Lead-Induced SCC of Alloy 690," pp. 208–215.
- H. Takamatsu et al., "Study on Lead-Induced Stress Corrosion Cracking of Steam Generator Tubing Under AVT Water Chemistry Conditions," pp. 216–223.
- G. Sui et al., "Stress Corrosion Cracking of Alloy 600 and Alloy 690 in Hydrogen/Steam and Primary Side Water," pp. 274–281.
- M. J. Psaila-Dombrowski et al., "Evaluation of Weld Metals 82, 152, 52 and Alloy 690 Stress Corrosion Cracking and Corrosion Fatigue Susceptibility," pp. 412–421.
- I. Bobin-Vastra, "Preoxidation of SG Alloy 690 Tubes to Decrease Metal Loss in the Primary Circuit: A Laboratory Study," pp. 507–513

APPENDIX B
REQUEST TO USE ALTERNATIVE TO ASME CODE THE EMBEDDED FLAW REPAIR TECHNIQUE

B.1 IDENTIFICATION OF COMPONENTS

Control rod drive mechanism (CRDM) penetrations and a head vent penetration on the upper reactor vessel head, which are ASME Class 1 components. There are between 50 and 100 head penetrations per reactor vessel.

B.2 CURRENT CODE REQUIREMENTS

ASME Section XI, 1989 edition, paragraph IWA-4120 specifies the following:

> "Repairs shall be performed in accordance with the Owner's Design Specification and the original Construction Code of the component or system. Later Editions and Addenda of the Construction Code or of Section III, either in their entirety or portions thereof, and Code Cases may be used."

Consequently, the proposed repairs will be conducted in accordance with the appropriate edition of ASME III and the alternative requirements proposed below.

B.3 CODE REQUIREMENTS FOR WHICH ALTERNATIVES ARE REQUESTED

Each Unit which requests the use of this relief will file a separate relief request, identifying the code edition and addenda which they are using, as well as their specific geometry. As an example, the 1989 code requirements are discussed below.

Per Section XI, 1989 edition, paragraph IWA-4120, repairs, if required, would be performed in accordance with Section III. Prior to welding, the repair excavation would require examination per paragraph NB-4453 with the acceptance criteria of NB-5351 and NB-5352. In neither case would it be permissible to weld over, or embed, an existing flaw.

Specifically, alternatives are being proposed for the following parts of ASME Section III, NB-4453:

NB-4453.1 addresses defect removal and requires liquid penetrant or magnetic particle examinations of the repair excavation with acceptance criteria per NB-5340 or NB-5350. In the proposed cases defects will not be removed. Instead, it is proposed that the defects be embedded with a weld overlay which will prevent further growth of the defects by isolating them from the reactor coolant which might cause them to propagate by primary water stress corrosion cracking (PWSCC). Structural integrity of the affected vessel head penetration J-groove weld will be maintained by the remaining unflawed portion of the weld.

NB-4453.2 discusses requirements for welding material, procedures, and welders. The requirements of this part will be satisfied by the proposed embedded flaw repair process.

NB-4453.3 requires that the repaired areas be uniformly blended into the surrounding surface. The proposed repairs will satisfy this requirement.

NB-4453.4 stipulates that the repairs be examined in accordance with requirements for the original weld. In the proposed cases where excavation of the original weld has occurred, the repairs will be subject to progressive liquid penetrant examination per the requirements of NB-5245. If no excavation has occurred prior to repair welding so that a temper bead procedure is not required, the weld overlay will be examined by liquid penetrant on the final surface. In both cases acceptance criteria will be per NB-5350.

NB-4453.5 requires the repairs be post weld heat treated per NB-4620. In the proposed cases, for repairs in the excavations that would require PWHT per NB-4620, a temper bead welding procedure will be used instead. Repairs where the remaining thickness of original weld buttering and/or the existing cladding maintain at least 1/8 inch between the overlay weld and the ferritic base material will not require PWHT per NB-4620.

Article IWB-3600, "Analytical Evaluation of Flaws" is not applicable to the proposed embedded flaw repairs because it contains no acceptance criteria for the components and material type in question. As a consequence the industry has proposed and the NRC has previously accepted criteria discussed in WCAP-13565, Rev. 1, for Westinghouse plants, and in Reports CEN 607 and CEN 614, for Combustion Engineering designed plants. We do not believe paragraphs IWB-3132 and IWB-3142 are applicable to the proposed embedded flaw repairs because these paragraphs discuss requirements related to Code imposed examinations, as is clear from their location in sub-subarticle IWB-3130, "Inservice Volumetric and Surface Examinations." The examinations that are being performed which may occasion the need to perform embedded flaw repairs are in excess of the Code mandated inspection for the reactor head penetrations and attachment welds. As stated in the body of the relief request, the inservice examination requirements of Table IWB-2500-01 mandate a visual examination from above the insulation for 25% of the penetration welds with IWB-3522 as the acceptance standard. There is no ISI requirement for the penetration tubes or repairs to them. As a consequence of the inapplicability of paragraphs IWB-3132 and IWB-3142 it is concluded that sub-subarticle IWB-2420 dealing with successive inspections is not applicable either since it specifically discusses flaw evaluations performed in accordance with IWB-3132.4 or IWB-3142.4.

B.4 BASIS FOR RELIEF

A request to use the embedded flaw technique to repair cracks on the inside diameter (ID) of control rod drive mechanism (CRDM) penetration tubes was previously submitted and approved by the NRC on a plant specific basis (see references 2, 12, 13, 14, and 15).

A request to use the embedded flaw technique to repair cracks on the outside diameter (ID) of control rod drive mechanism (CRDM) penetration tubes as well as repair of cracks on the J-groove attachment welds of these penetrations has also been previously submitted and approved by the NRC on a plant specific basis.

The 1995 Edition of Section XI with 1996 Addendum, subparagraph IWA-46.11, permits the use of Section XI flaw evaluation criteria which would not require the complete removal of a flaw unless repairs were being undertaken per the temper bead welding procedures of paragraph IWA-4620, or paragraphs

IWA-4630 and IWA-4640 with the flaw penetrating the base metal. The flaw evaluation criteria of Section XI (refer to Table IWB-3514-2) establishes acceptance criteria for surface connected and embedded flaws.

A number of PWR plant owners will perform inspections under the insulation of the reactor vessel head during upcoming refueling outages. If the inspections identify any penetration nozzle leakage, additional under the head inspections will be performed. In the event that any subsequent under the head inspections of the reactor vessel head penetrations reveal flaws in those penetrations, it will be necessary to repair the flaws that exceed Section XI acceptance criteria. This relief request will permit any flaws identified on reactor vessel head penetrations and on J-groove attachment welds to be evaluated utilizing criteria documented in WCAP-13998, Revision 1, "RV Closure Head Penetration Tube ID Weld Overlay Repair," (Reference 2) and repaired using an embedded flaw repair technique.

The embedded flaw repair technique is considered a permanent repair lasting through plant life extension for a number of reasons: first, as long as a Primary Water Stress Corrosion Cracking (PWSCC) flaw remains isolated from the primary water (PW) environment, it cannot propagate. Since Alloy 52 (690) weldment is considered highly resistant to PWSCC, a new PWSCC crack should not initiate and grow through the Alloy 52 overlay to reconnect the PW environment with the embedded flaw. The resistance of the alloy 690 material has been demonstrated by laboratory testing for which no cracking of the material has been observed in simulated PWR environments, and in approximately 10 years of operational service in steam generator tubes, where likewise no PWSCC has been found.

Therefore, the embedded flaw repair technique is considered to be an alternative to Code requirements that provides an acceptable level of quality and safety, as required by 10 CFR 50.55a(a)(3)(i).

B.5 ALTERNATE REQUIREMENTS

The proposed repairs will involve one of two approaches. For cases where the J-groove weld has been partially excavated either to obtain a "boat" sample for analysis or in conjunction with previously undertaken flaw exploration, the excavation will be rewelded with Alloy 52 flush with the existing weld surface, using a temper bead weld technique if necessary. These repairs will be examined by progressive liquid penetrant inspection. The entire weld will then be overlaid with three weld passes of Alloy 52 weld material. For cases where no weld excavation has occurred, the existing weld will also be overlaid with three weld passes of Alloy 52 material. All final weld surfaces will be liquid penetrant inspected.

Per the 1986 Edition of ASME Section XI, paragraph IWB-2200(a), no preservice examination is required for repairs to the partial penetration J-grove welds between the vessel head and its penetrations (Examination Category B-E) or for the penetrations themselves. However, the NDE performed after welding will serve as a preservice examination record as needed in the future. Furthermore, the inservice inspection requirements from Table IWB-2500-1, "Examination Category B-E...," is a VT-2 visual inspection of the external surfaces of 25% of the nozzles each interval with IWB-3522 as the acceptance standard. There are no ISI requirements for the penetration tubes or repairs to the tube. Currently, we perform visual examination, VT-2, of 100% of the nozzles each refueling outage. Ongoing vessel head penetration inspection activities undertaken as a result of NRC Bulletin 2001-01 and ongoing deliberations in Code committees will be monitored to determine the necessity to perform any additional or augmented inspections.

Relative to the need for successive examinations in accordance with IWB-2420, we have concluded that no such examinations are required by the Code, as discussed above. Regardless of the applicability of the ASME Code article, it is important to ensure that the repair is effective in isolating the cracking from the PWR environment permanently. The first step in ensuring this is the choice of a weld material not susceptible to PWSCC, which has been done with the Alloy 52 weldment. After the weld repair is completed, its integrity is verified by liquid penetrant inspection. There are no known mechanisms for any further potential cracking of the weld used to embed the flaw, or the surrounding region, except for fatigue. As mentioned earlier, the calculated fatigue usage in this region is very low, because the reactor vessel head region is isolated from the transients which affect the hot leg or cold leg piping. The thickness of the weld has been set to provide a permanent embedment of the flaw, without adding sufficient weld to increase the residual stresses. This ensures that the embedded flaw repair will not affect areas nearby to the repair.

Therefore, there is no need for follow-up inspections of the repaired area from a technical point of view. However, it is considered prudent to demonstrate the effectiveness of the repairs. Therefore, for the proposed embedded flaw repairs involving the J-groove weld, an ultrasonic examination of the OD of the penetration immediately above the weld will be performed in the next inspection period to verify that no OD connected circumferential flaws exist. Also, a liquid penetrant inspection or eddy current exam of any weld overlays will be performed.

Using the provisions of this request relief as an alternative to Code requirements will produce sound, permanent repairs and an acceptable level of quality and safety, as required by 10 CFR 50.55a(a)(3)(i).

Appendix C
Embedded Flaw Repair Analytical Basis For a Typical Plant

APPENDIX C
EMBEDDED FLAW REPAIR ANALYTICAL BASIS FOR A TYPICAL PLANT

C.1 INTRODUCTION

C.1.1 Background

Cracking has been observed in the Alloy 600 reactor vessel head adapter penetration nozzles for a number of plants. In one case, a leak resulted from a through-wall flaw. The cracks have been determined to result from Primary Water Stress Corrosion Cracking (PWSCC) in the nozzles, and have led to requests for inspections of these regions. The cracks have been attributed to the residual stresses, induced by the ovality and the bending of the penetration nozzle, introduced by the attachment weld or J-groove weld. As a result of the Alloy 600 vessel head penetration cracking issue, the embedded flaw repair approach has been developed by Westinghouse to assist the utilities in determining repair strategies in the event that future reactor vessel head penetration inspections identify indications in the penetration nozzles.

C.1.2 Embedded Flaw Repair Approach

The embedded flaw repair technique was developed by Westinghouse in 1994, and involves the deposition of two or three layers of Alloy 52 weld metal to isolate existing flaws and susceptible material from the primary water environment. The embedded flaw repair technique is considered a permanent repair and provides a non-structural barrier to the area of interest to stop the corrosion process. As long as a crack remains isolated from the Primary Water environment, PWSCC will not occur. Since Alloy 52 weldment is resistant to PWSCC, a new PWSCC type of crack should not initiate and grow through the Alloy 52 overlay to permit the environment to come in contact again with the susceptible material. The resistance of Alloy 690 and its associated welds, Alloys 52 and 152, has been demonstrated by laboratory testing in which no cracking has been observed in simulated Pressurized Water Reactor (PWR) environments, and by over 10 years of operational service in steam generator tubes, where no PWSCC has occurred. The crack growth resistance of this material has been documented in Appendix A.

The residual stresses produced by the embedded flaw technique have been measured and found to be relatively low because of the small weld overlay thickness. This implies that no new cracks will initiate and grow in the area adjacent to the repair weld. There are no other known mechanisms for significant crack propagation in this region because the cyclic fatigue loading is considered negligible. The Cumulative Usage Factor (CUF) in the upper head region was calculated to be typically less than 0.2 in reactor vessel design reports, as well as in various aging management review reports.

Editions of ASME Code Section XI prior to 1992, do not permit welding over an existing flaw, so the embedded flaw repair requires a relief request. In the fall of year 2000, surface flaws were first found on the outside diameter of head penetration nozzles, as well as in the attachment welds. These locations are equally amenable to the embedded flaw repair.

For plants using the 1992 code or later editions and addenda, the repair requirements of IWA 4300 do allow welding over an existing crack, provided that the crack is accepted "in accordance with the

appropriate flaw evaluation rules of Section XI." This provides an alternative approach for plants that might not want to ask for relief in order to employ an embedded flaw repair. In this case, a series of analyses could be performed to identify the maximum flaw sizes acceptable to the criteria of section XI. Such evaluations would have to consider flaws in the head penetrations themselves, as well as the attachment welds. These evaluations have come to be termed IWB 3600 evaluations or embedded flaw repair evaluation, and have been performed for a number of plants. The evaluation to be summarized herein provides the basis for the embedded flaw repair, for a typical plant.

C.1.3 Penetration Nozzle Geometry

The embedded flaw repair technique is intended for application to reactor vessel head penetrations designed by Westinghouse and Combustion Engineering. The Control Rod Drive Mechanism (CRDM) and Control Element Drive Mechanism (CEDM) nozzles have similar geometries, with an outer diameter ranging from 3.50 to 4.25 inches for CEDMs, and a constant outer diameter of 4.0 inches for CRDMs. The inside diameter (ID) of the CEDMs ranges from 2.718 to 2.728 inches, while the CRDMs have a constant inside diameter of 2.75 inches. Most Combustion Engineering designs also have In Core Instrumentation (ICI) penetrations in the upper head regions. The outside diameter (OD) of the ICI penetrations ranges from 4.5 inches to 6.625 inches. The inside diameter of these nozzles ranges from 3.625 to 5.19 inches. A sketch of the typical vessel head penetration nozzle configuration is shown in Figure C.1-1.

C.1.4 Overall Approach

Westinghouse has developed the following three repair scenarios/methods to address the most common types of flaws found during the vessel head inspection. The embedded flaw repair method provides a non-structural fluid barrier to the area of interest in order to stop the corrosion process.

Scenario # 1 - Axial or Circumferential Crack in the Penetration ID

Scenario # 2 - Axial Crack in the Penetration J-Weld

Scenario # 3 - Axial Crack on the Penetration Nozzle OD (Below the J-Weld)

Scenarios 1 through 3 require increased excavation and/or weld overlays. The analytical methods required prior to implementation of these repair scenarios/methods are addressed in Sections C.2.0 to C.4.0.

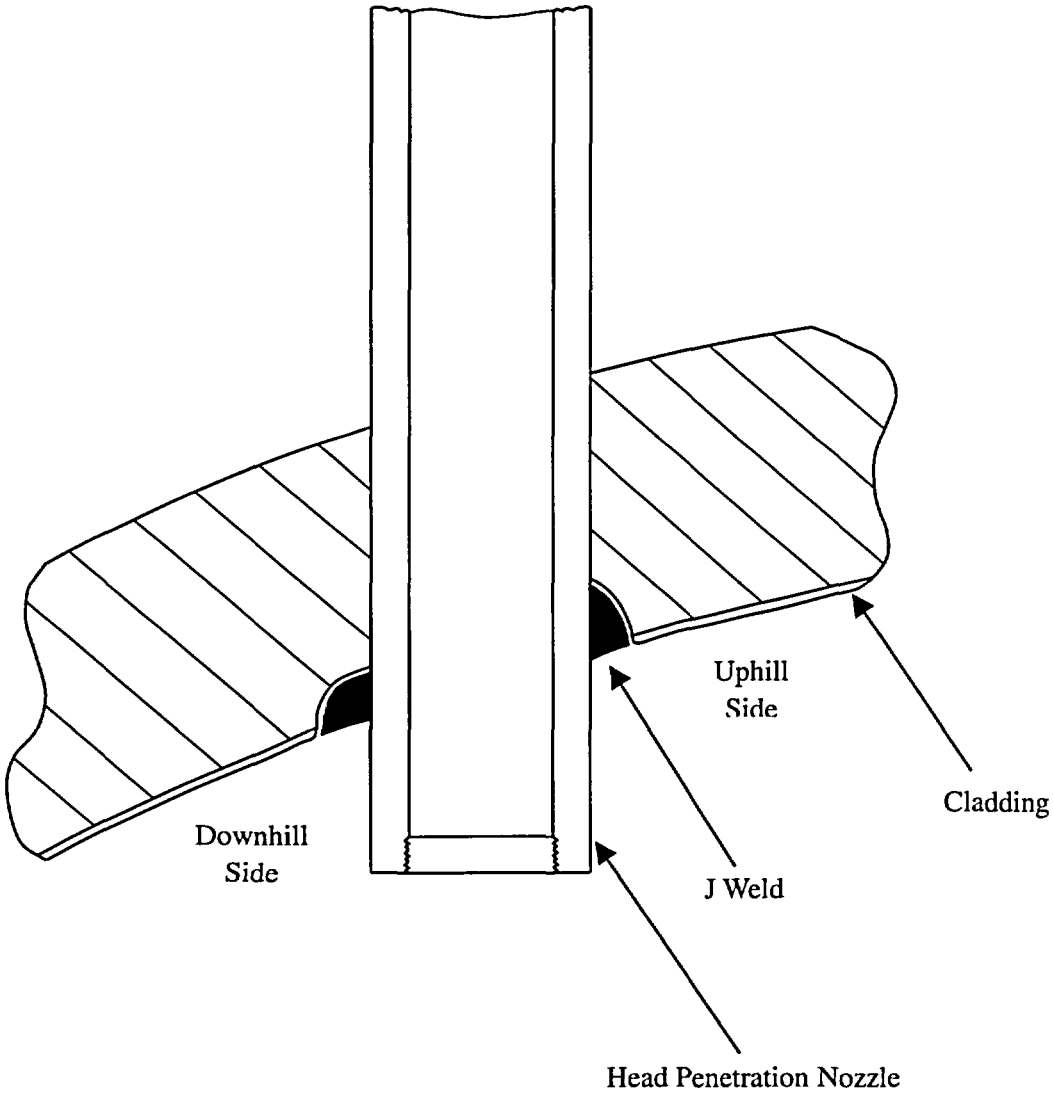

Figure C.1-1 Typical Configuration of a Vessel Head Penetration Nozzle

C.2 SCENARIO # 1 - AXIAL OR CIRCUMFERENTIAL CRACK IN THE PENETRATION ID

[

]^{a,c,e} Flaw evaluations for postulating planar flaws with various flaw depths in the head penetration nozzles were performed to determine the largest flaw size that can be repaired using the embedded flaw repair technique, and maintaining ASME Code margins.

C.2.1 Methodology

The evaluation assumed that a flaw has been detected in a penetration nozzle and that the embedded flaw repair method is used to isolate the flaw from further exposure to the primary water environment. The evaluation began with the determination of an allowable flaw size discussed in Section C.2.2 for a flaw postulated in the penetration nozzle. [

]^{a,c,e} The reduced allowable flaw size was then used as the maximum allowable flaw size that can be tolerated using the embedded flaw repair method.

The evaluation procedures and acceptance criteria for indications in austenitic piping are contained in paragraph IWB 3640 of ASME Section XI [1]. These criteria have remained unchanged through the 1992 Edition. [

]^{a,c,e}

C.2.2 Allowable Flaw Size

The requirement for evaluation of a flaw using the rules of Section XI is that the governing transients be chosen from the normal/upset conditions as well as from the emergency/faulted conditions.

[

]^{a,c,e}

C.2.2.1 Allowable Flaw Sizes for Embedded Axial Flaws

[

]^{a,c,e}

[

]a,c,e

IWB 3600 Acceptance Criteria for Axial Flaws

[

]a,c,e

[

]^{a,c,e}

C.2.2.2 Allowable Flaw Sizes for Embedded Circumferential Flaws

[It is understood that the allowable flaw size for surface flaws envelops that for the embedded flaws of comparable size, therefore to determine the allowable flaw size for an embedded circumferential flaw, the allowable limit stress must first be calculated using the acceptance criteria discussed below for a range of semi-elliptical circumferential surface flaws postulated on the inside surface of the penetration nozzles.

IWB 3600 Acceptance Criteria for Circumferential Flaws

For circumferential flaws, the longitudinal membrane stress is calculated from internal pressure and axial components of other loads on the penetration nozzle. The longitudinal primary membrane stress at limit load under pure membrane loading, σ_m^c, is calculated by using the following expression:

and

where:

θ = Half Flaw Angle

σ_f = Flow Stress for the penetration nozzle material

The allowable primary membrane stress, S_t, is then given by

]^{a,c,e}

[

]^{a,c,e}

C.2.3 Fatigue Crack Growth Prediction

The analysis procedure involves postulating an initial flaw in the penetration nozzle and calculating the crack growth due to an imposed series of loading transients. For the fatigue crack growth prediction, the effects of secondary stresses resulting from thermal transient and residual stresses must be considered.

C.2.3.1 Thermal Transients

The design basis thermal transients and cycles are used for calculation of the fatigue crack growth. These thermal transients are designed in the applicable equipment specifications.

C.2.3.2 Finite Element Analysis Stress Data

There are many head penetration nozzles in the reactor vessel upper head. The outermost head penetration nozzles were selected for analysis because the [

]^{a,c,e} The distributions of residual, transient thermal, and pressure stresses in the vessel head penetration nozzle were obtained from detailed three-dimensional elastic-plastic finite element analyses based on the loadings discussed in Section C.2.3.1. The finite element stress analysis results performed for a typical plant was used. [

]^{a,c,e} The finite element model with the selected stress cuts is shown in Figure C.2-4. Stress Cuts 3 and 6 are used because the regions of the head penetration that have the highest stresses are the ones closest to the attachment weld.

C.2.3.3 Stress Intensity Factor

One of the key elements in the fatigue crack growth evaluation is the determination of the crack driving force or stress intensity factor (K_I). This is based on the equations available in the literature discussed below.

Stress Intensity Factor for Surface Flaw

For a part-through wall flaw, the stress profile is approximated by a cubic polynomial as follows:

$$\sigma(x) = A_0 + A_1 x + A_2 x^2 + A_3 x^3$$

where:

x	=	The Distance into the wall (inch)
σ	=	Stress Perpendicular to the plane of the Crack (ksi)
A_i	=	Coefficients of the Cubic Polynomial Fit, i = 0, 1, 2, 3

For a surface flaw in the penetration nozzle, the stress intensity factor expression of Raju and Newman [2] is used.

Stress Intensity Factor for Embedded Flaw

The stress intensity factor expression for an embedded flaw is described in Appendix A-3000 of ASME XI.

The stress intensity factor range, ΔK_I, that controls fatigue crack growth, depends on the geometry of the crack, its surrounding structure and the range of applied stresses in the region of the postulated crack. Once ΔK_I is calculated, the fatigue crack growth due to a particular stress cycle can be determined using a crack growth rate reference curve applicable to the material of the head penetration nozzle.

C.2.3.4 Crack Growth Rate

[

]^{a,c,e}

Once the incremental crack growth is calculated, it is then added to the original crack size, and the analysis proceeds to the next cycle and/or thermal transient. The procedure is repeated in this manner until all the significant analytical thermal transients and cycles known to occur in the 10, 20, 30 or 40 years of operation have been analyzed. The cycles are distributed evenly over the entire plant design life.

C.2.4 Maximum Allowable Flaw Size

Allowable flaw sizes determined as discussed in Section C.2.1 were adjusted to account for the fatigue crack growth of the repaired flaws, which are embedded and free from stress corrosion cracking. These embedded flaws are the result of repairing the axial and circumferential part-through flaws on the inside surface of the penetration nozzles using the embedded flaw repair method. The amount of adjustment is based on the fatigue crack growth analysis results described in Section C.2.3.

Maximum Allowable Flaw Sizes for Embedded Axial Flaws

For illustration purposes, Figure C.2-5 present the maximum allowable flaw sizes for the embedded axial flaws in the head penetration nozzles along with the ASME Code based allowable flaw depths and shapes discussed in Section C.2.1. The results have incorporated the effects of fatigue crack growth.

Maximum Allowable Flaw Sizes for Embedded Circumferential Flaws

For illustration purposes, Figure C.2-6 presents the maximum allowable flaw sizes for the embedded circumferential flaws in the head penetration nozzles along with the ASME Code based allowable flaw depths and shapes discussed in Section C.2.1. The results have incorporated the effects of fatigue crack growth.

a,c,e

Figure C.2-1 Axial or Circumferential Crack in the Penetration Tube ID

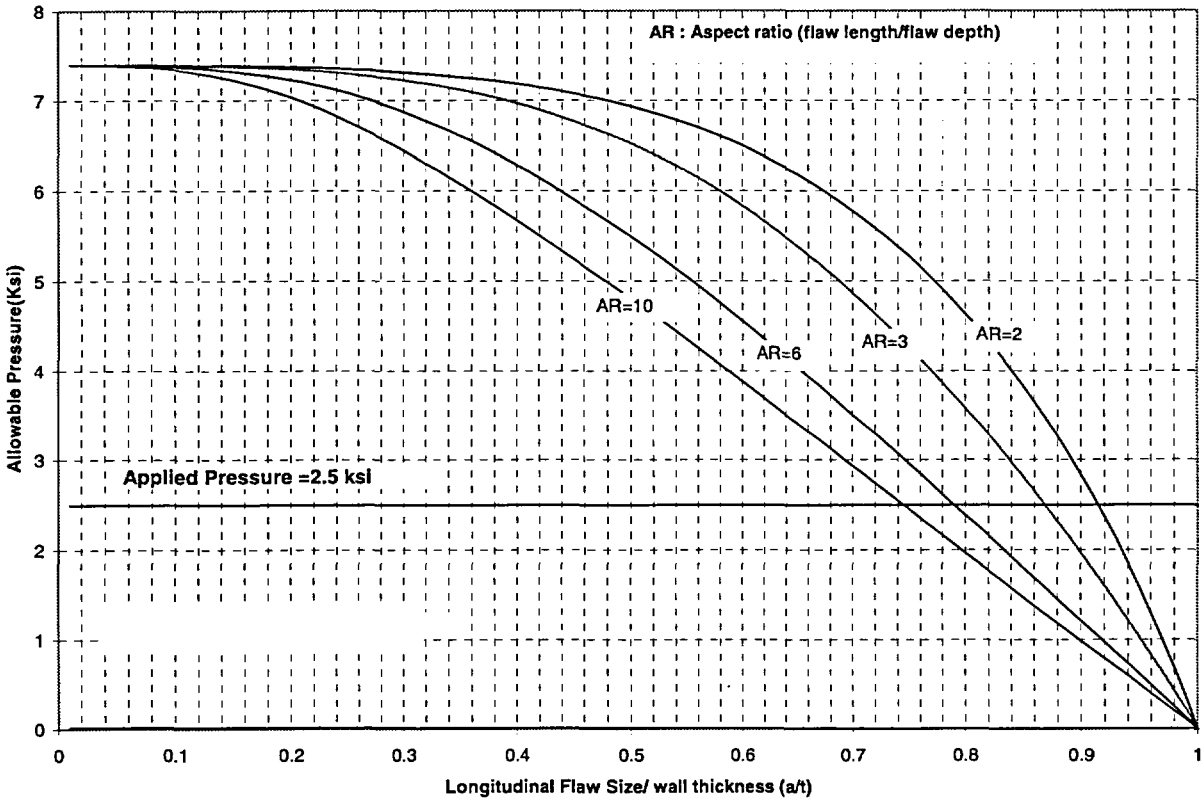

Figure C.2-2 Determination of Allowable Axial Flaw Sizes

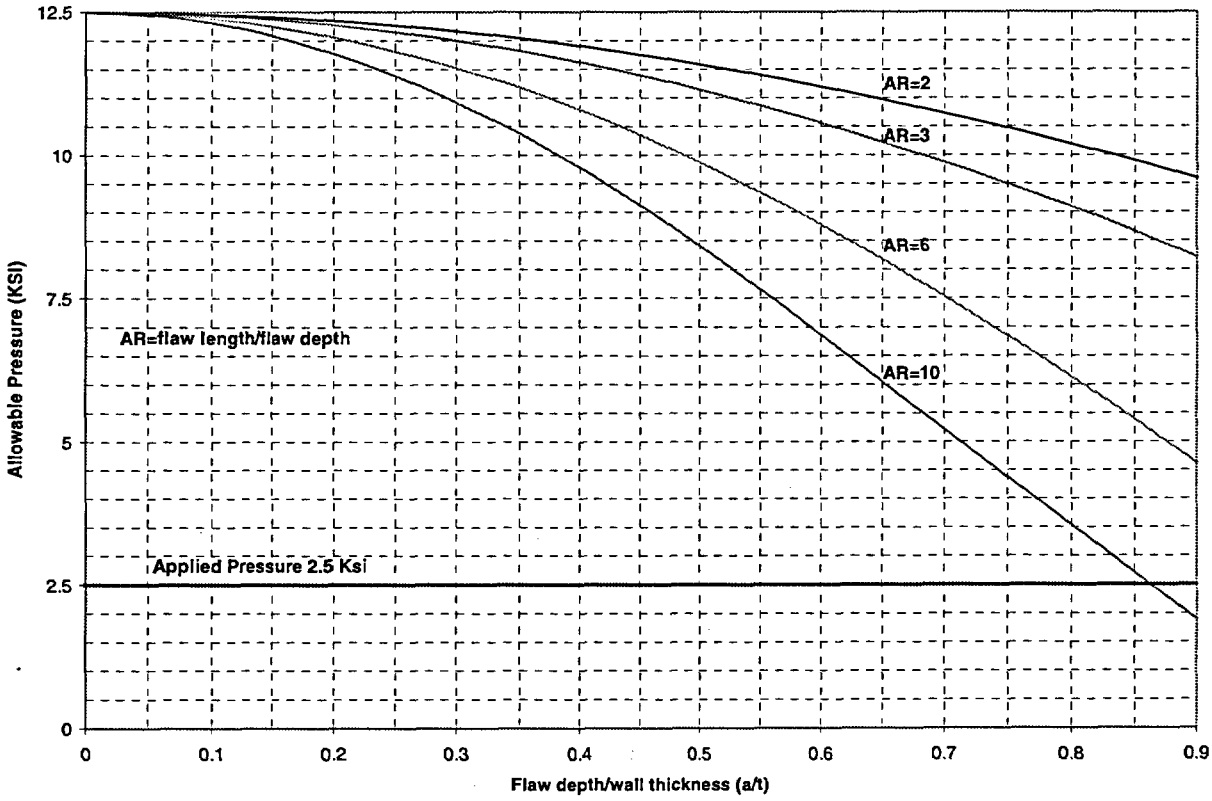

Figure C.2-3 Determination of Allowable Circumferential Flaw Sizes

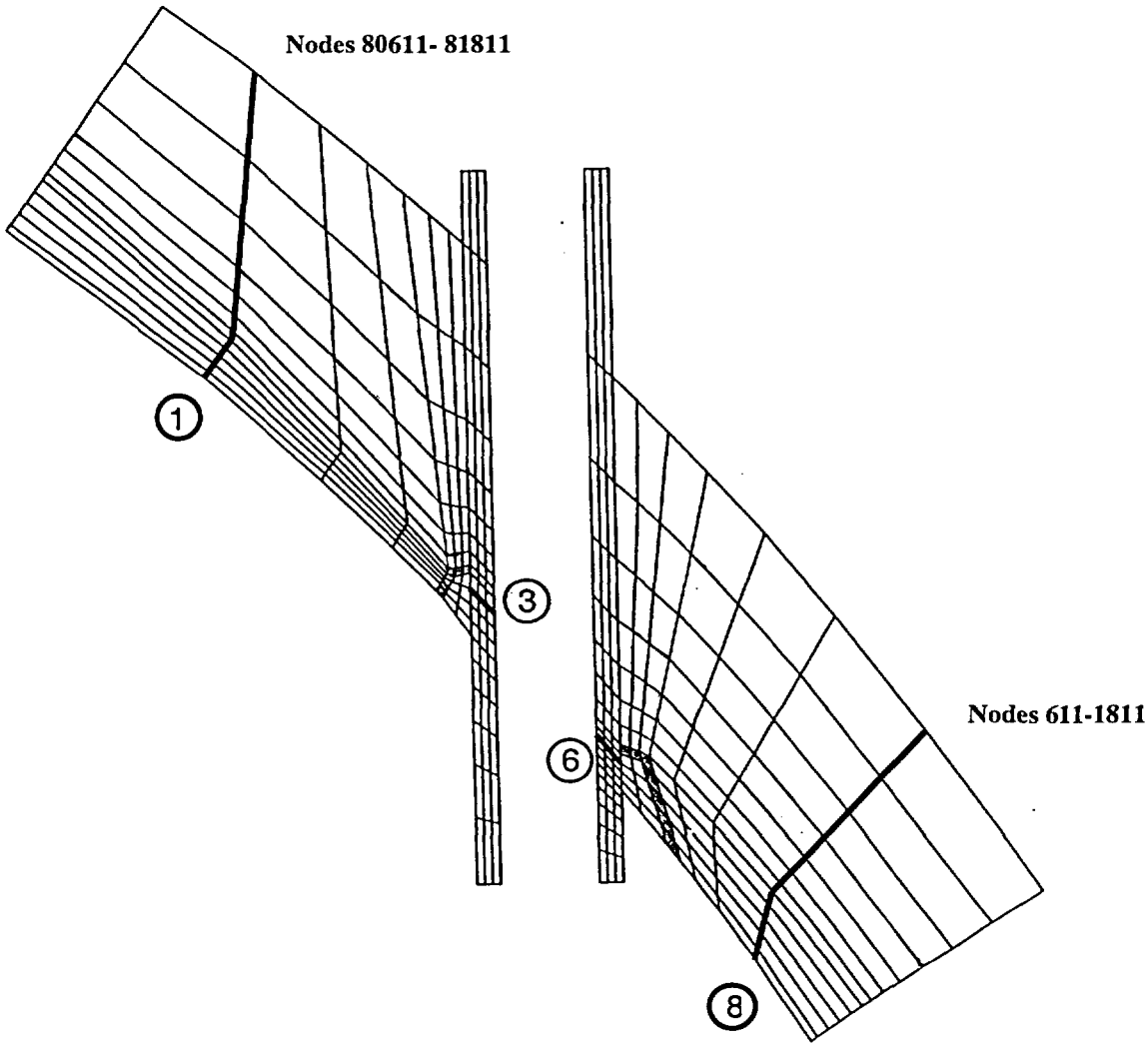

Figure C.2-4 Finite Element Model with Selected Stress Cuts

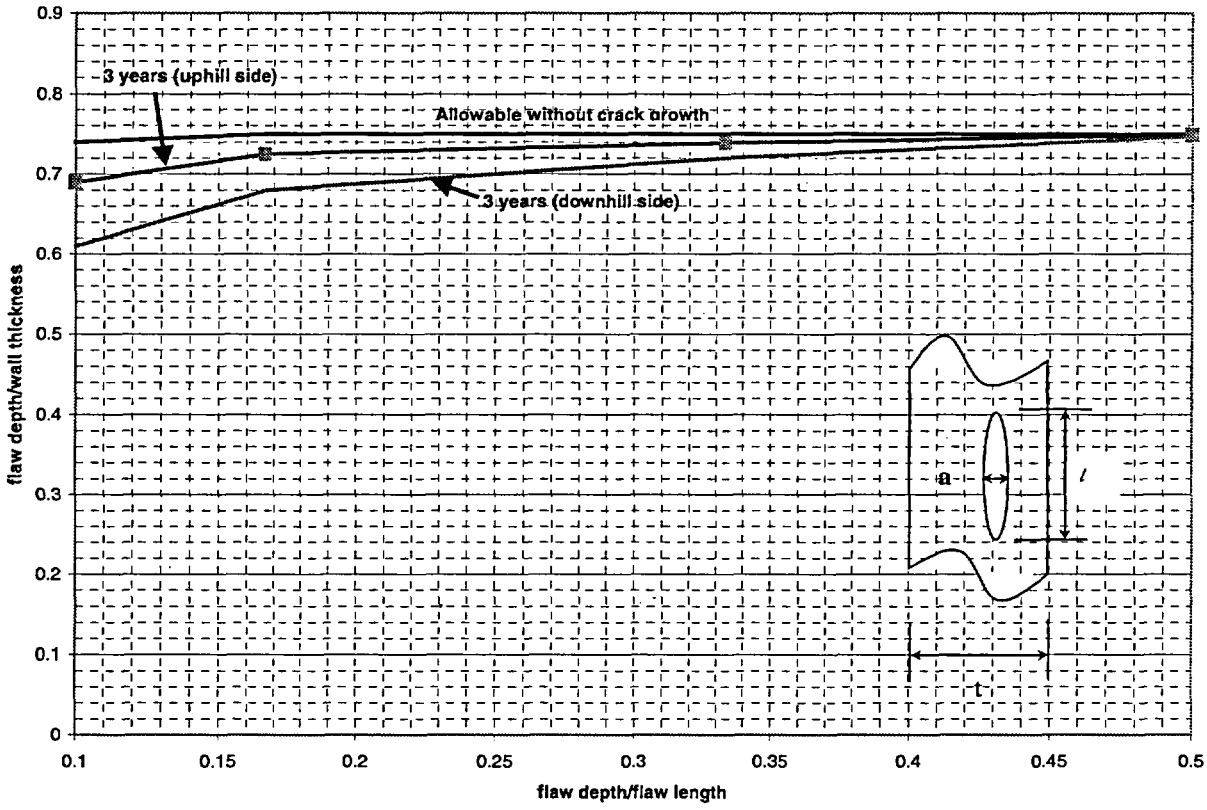

Figure C.2-5 Maximum Allowable Embedded Axial Flaw Sizes

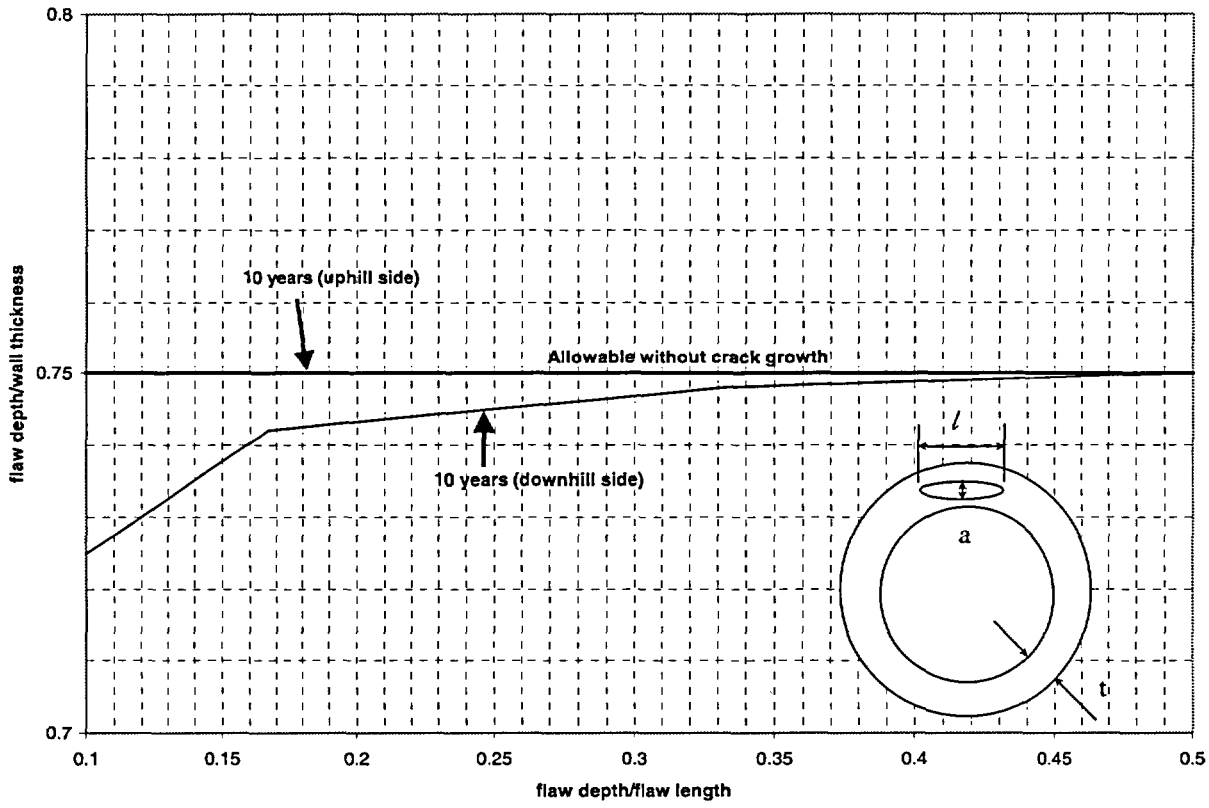

Figure C.2-6 Maximum Allowable Embedded Circumferential Flaw sizes

C.3 SCENARIO # 2 –AXIAL CRACK IN THE PENETRATION J-WELD

[

]^{a,c,e}

C.3.1 Methodology

The evaluation assumed that a flaw has been detected in a penetration nozzle attachment weld and that the embedded flaw repair method is used to seal the flaw from further exposure to the primary water environment. [

]^{a,c,e}. With the embedded flaw repair method, the only mechanism for sub-critical crack growth is due to fatigue. The allowable flaw size is therefore adjusted for the predicted fatigue crack growth to obtain the maximum allowable flaw size that can be repaired in the attachment weld using the embedded flaw repair method.

C.3.2 Allowable Flaw Size

The evaluation began with the determination of an allowable axial flaw size based on the acceptance criteria described below for a postulated axial flaw in the vessel head near the penetration nozzle that encompassed the entire attachment weld region. Figure C.3-2 illustrates the use of the following acceptance criteria in determining the allowable flaw size.

C.3.2.1 Acceptance Criteria – Linear Elastic Fracture Analysis

The methodology used is consistent with the flaw evaluation procedures of Section XI in the Code, as embodied in IWB 3600 of Section XI. The acceptance criteria are based on that provided in the flaw evaluation process of paragraph IWB 3600. There are two alternative sets of flaw acceptance criteria for continued service without repair in paragraph IWB-3600. Either of the criteria below may be used.

- Acceptance Criteria Based on Flaw Size (IWB-3611)
- Acceptance Criteria Based on Stress Intensity Factor (IWB-3612)

Both criteria are comparable for thick-wall sections, and the acceptance criteria based on stress intensity factor have been determined by past experience to be less restrictive for many cases.

Acceptance Criteria Based on Stress Intensity Factor

The term stress intensity factor (K_I) is defined as the driving force on a crack. It is a function of crack size and the applied stresses, as well as the overall geometry of the structure. In contrast, the fracture toughness (K_{Ia}, K_{Ic}) is a measure of the resistance of the material to crack propagation. Fracture toughness as discussed in Section C.3.2.3 is a material property and is also a function of temperature.

The acceptance criteria for the stress intensity factor (K_I) are:

$$K_I < \frac{K_{Ia}}{\sqrt{10}}$$ For normal conditions (upset and test conditions inclusive)

$$K_I < \frac{K_{Ic}}{\sqrt{2}}$$ For faulted conditions (emergency conditions inclusive)

where:

K_I = The maximum applied stress intensity factor for a flaw size a_f, to which a detected flaw will grow, during the conditions under consideration, for a specified period, or to the next inspection

K_{Ia} = Fracture toughness based on crack arrest for the corresponding crack tip temperature

K_{Ic} = Fracture toughness based on crack initiation for the corresponding crack tip temperature

To determine whether a flaw is acceptable for continued service without repair, both criteria for the stress intensity factor must be met.

C.3.2.2 Acceptance Criteria – Elastic Plastic Fracture Analysis

As part of an effort to quantify the margins available in reactor pressure vessels, the ASME Section XI Working Group on Flaw Evaluation developed elastic-plastic fracture evaluation procedures in the early 1980s. These procedures were documented in Welding Research Council Bulletin 413 [6], and were implemented in Appendix K of Section XI. Appendix K, and its predecessor, Code Case N-512, appeared in their final form in 1995.

Although the original purpose of Appendix K was evaluation of reactor vessels with low upper shelf fracture toughness, the methods are equally applicable to any region of the reactor vessel where the fracture toughness can be described with elastic plastic parameters. The head region of the reactor vessel is the hottest portion of the reactor vessel where the steady state temperature is approximately 550-600 °F. This ensures ductile behavior, and so the use of elastic-plastic methods is appropriate.

This approach to the integrity of a nuclear vessel has been developed over a ten-year period, and has been illustrated with a number of example problems [6] to demonstrate its use. The extension of this methodology to issues other than the low shelf fracture toughness issue is appropriate when service

conditions (temperature) ensure ductile behavior. The extension of the Elastic Plastic Fracture Mechanics (EPFM) method to the reactor vessel head is appropriate, as discussed above.

The acceptance criteria are to be satisfied for each category of transients, namely, Service Load Levels A and B (normal and upset). Level C (emergency) and Level D (faulted) conditions. The criteria are listed below:

$$J < J_{0.1}$$

$$\frac{\partial J}{\partial a} < \frac{dJ_R}{da}$$

J_R = The J-integral resistance to ductile tearing for the material.

J_I = The applied J-integral.

$J_{0.1}$ = The J-integral resistance at a ductile flaw extension of 0.1 inch.

$\frac{\partial J}{\partial a}$ = is the partial derivative of the applied J-integral with respect to flaw depth a.

$\frac{dJ_R}{da}$ = is the slope of the J-R curve.

The J-integral fracture resistance of the material can be determined using the Regulatory Guide 1.161[7].

As suggested by Appendix K, the J-integral due to applied loads has been evaluated using the crack tip stress intensity factor with a plastic zone correction. The flaw depth at which the calculation is made is equal to this postulated flaw depth plus 0.1 inches. In Appendix K, the postulated flaw depth is set at one quarter the wall thickness, but in this case the postulated flaw size is that of the attachment weld.

The results using the elastic plastic fracture method are shown in Figure C.3-6. The key aspect of the analysis is the slope of the J-material curve and the slope of the J-applied curve. At a crack extension of 0.1 inch, the slope of the J-material curve far exceeds the slope of the J-applied curve, demonstrating that the flaw is stable. Therefore, this approach will demonstrate increased margin compared to the LEFM approach of C.3.2.1.

C.3.2.3 Stress Intensity Factor Calculation

One of the key elements in using the above acceptance criteria is the determination of the crack driving force or stress intensity factor (K_I) for the postulated crack configuration in the penetration nozzle. This is based on the information available in the literature.

Stress Intensity Factor

The stress intensity factors for the postulated axial flaw in the attachment weld region of the penetration nozzles are based on that from the work by [ ]^{a,c,e}. The use of this stress intensity factor expression requires that the stresses remote from the hole be resolved into membrane and bending stress components. The stress intensity factor can be expressed conservatively in terms of the linearized membrane and bending stress components as follows:

[ ]^{a,c,e}

The [ ]^{a,c,e} is applicable for a range of flaw shapes, with the depth of the flaw defined as "a", and the width of the flaw defined as "ℓ", as shown in Figure C.3-3. This flexibility is necessary because this expression will be applied to a range of flaw shapes corresponding to different attachment weld shapes. The coefficients A and B can be found in Reference [4] for selected values of r/t, a/l and a/t, where "r" is the outside radius of the penetration nozzle and "t" is the wall thickness of the reactor vessel head. For the r/t, a/l and a/t values not shown in Ref. [4], the coefficients A and B were determined using interpolation. Since the coefficients are provided for a number of locations around the flaw front, [ ]^{a,c,e}.

Finite Element Stress Data

There are many head penetrations in the reactor vessel upper head, and the highest stressed region of the vessel head is chosen for analysis to determine the membrane and bending stress components in the stress intensity factor calculation. The distribution of residual, transient thermal, and pressure stresses in the closure head region is obtained from detailed three-dimensional elastic-plastic finite element analyses of the head penetration nozzle region using iso-parametric finite elements. The thermal transients used are consistent with those used in the fatigue crack growth calculation discussed in Section C.3.3.

Two stress cuts 1 and 8 were selected for the analysis, one on the uphill side of the outermost penetration nozzle and the other one on the downhill side. The finite element model with the selected stress cuts is shown in Figure C.3-4. The resulting through-wall stress distributions from these stress cuts were used to determine the membrane and bending stress components required to determine the stress intensification factor. These stress cuts are chosen to be more than one penetration nozzle diameter away from the penetration nozzle to ensure that the stress concentration effects of the hole in the vessel head are minimized. This is because stresses without stress concentration are needed in calculating the stress intensity factor using Ref. [4].

Fracture Toughness

The other key element in the above acceptance criteria is the fracture toughness of the material. The fracture toughness has been taken directly from the reference curves in [

]^{a,c,e}.

The value of RT_{NDT} which is a parameter determined from Charpy V-notch and drop-weight tests is used in the determination of the fracture toughness. Neutron irradiation has been shown to produce embrittlement that reduces the toughness properties of reactor vessel ferritic steel material. The irradiation levels are very low in the reactor vessel head region and therefore the fracture toughness will not be measurably affected.

The upper shelf temperature regime requires utilization of a upper shelf toughness that is not specified in the ASME Code. A value of 200 $ksi\sqrt{in}$ has been used here since the upper shelf Charpy energy exceeds 50 ft-lb even after irradiation. This value is consistent with the general practices in this kind of evaluations, as demonstrated in Ref. [5], which provides the background and technical basis of Appendix A of Section XI.

C.3.3 Fatigue Crack Growth Prediction

The analysis procedure involves postulating an initial flaw in the penetration nozzle attachment weld region and calculating the crack growth due to the transients. For the fatigue crack growth prediction, the effects of secondary stresses resulting from thermal transient and residual stresses must be considered.

Two stress cuts 2 and 7 near the penetration nozzles were selected for the analysis, one on the uphill side of the outermost penetration nozzle and the other one on the downhill. The finite element model with the selected stress cuts is shown in Figure C.3-4. The resulting through-wall stress distributions from these stress cuts were used to determine the stress intensification factor for the postulated axial flaw in the attachment weld region based on the work of ASME XI, Appendix A-3000.

The stress intensity factor, ΔK_I, which controls the fatigue crack growth, depends on the geometry of the crack, its surrounding structure and the range of applied stresses in the region of the postulated crack. Once ΔK_I is calculated, the fatigue crack growth due to a particular stress cycle can be determined using a crack growth rate reference curve applicable to the material where the crack is postulated.

The crack growth rate curves used in the analyses are taken directly from [
]^{a,c,e} for fatigue crack growth into the vessel. Since the flaw is isolated from the primary water environment, the crack growth rate reference curve for the air environment is used. This curve is a function of the applied stress intensity factor range (ΔK_I) and the R ratio, which is the ratio of the minimum to maximum stress intensity factor during a thermal transient. [

]^{a,c,e}

[

]^{a,c,e}

Once the incremental crack growth is calculated, it is then added to the original crack size, and the analysis proceeds to the next cycle and/or thermal transient. The procedure is repeated in this manner until all the significant analytical thermal transients known to occur in 10, 20, 30, or 40 years of operation have been analyzed. The cycles of the transients used for this evaluation are distributed evenly over the plant design life.

C.3.4 Evaluation of Postulated Attachment Weld Shapes

The predicted fatigue crack growth discussed in Section C.3.3 was subtracted from the allowable flaw sizes calculated in Section C.3.2 to result in the maximum allowable flaw sizes as a function of flaw shape. The adjusted maximum allowable flaw sizes are illustrated in Figure C.3-5 for the head penetration attachment welds. In order to determine the acceptability of the postulated weld shapes in the attachment weld region of the vessel head penetration nozzles, the actual geometry of the attachment weld shapes is also plotted in Figure C.3-5. The results show that all the postulated head penetration nozzle attachment weld sizes and shapes are less than the allowable flaw sizes. Therefore, the results of the evaluation in Figure C.3-5 can be used to demonstrate that embedded flaw repair can be applied to the attachment welds from the inside surface of the vessel head regardless of the size of a flaw in the penetration nozzle attachment weld.

C.3.5 Fatigue Crack Growth into the Repair Weld

J-weld repair is performed by depositing three layers of Alloy 52 weld material onto the flawed J-weld. The flaw is thus sealed, and the thickness of the reactor vessel shell is locally increased by the weld overlay thickness. In the analysis, an embedded flaw is assumed. For a conservative analysis, it is assumed that the entire depth of the J-weld, which is of Alloy 182, is flawed. In other words, the postulated embedded flaw starts beneath the free surface and ends at the boundary of J-weld within reactor vessel head base metal. For conservatism, the aspect ratio of the embedded flaw is taken as 6.0.

For illustration purposes, the predicted fatigue crack growth for the postulated weld shapes is shown in Table C.3-1. The FCG prediction results indicate the repaired weld can last at least 12 years of service life.

Table C.3-1 Predicted Fatigue Crack Growth (inches) into the Repaired Attachment Welds (For illustration purposes only)

	Downhill Side		Uphill Side	
Yr.	Point 1 (inch)	Point 2 (inch)	Point 1 (inch)	Point 2 (inch)
0	0.1875	1.8110	0.1875	2.1260
1	0.1850	1.8118	0.1781	2.1291
2	0.1825	1.8126	0.1683	2.1322
3	0.1800	1.8134	0.1582	2.1353
4	0.1774	1.8141	0.1475	2.1383
5	0.1748	1.8149	0.1364	2.1413
6	0.1722	1.8157	0.1246	2.1444
7	0.1696	1.8165	0.1119	2.1474
8	0.1670	1.8173	0.0982	2.1503
9	0.1643	1.8181	0.0831	2.1533
10	0.1616	1.8188	0.0657	2.1563
11	0.1589	1.8196	0.0445	2.1592

Table 3-1 Predicted Fatigue Crack Growth (inches) into the Repaired Attachment Welds (Cont'd) (For illustration purposes only)				
	Downhill Side		Uphill Side	
Yr.	Point 1 (inch)	Point 2 (inch)	Point 1 (inch)	Point 2 (inch)
12	0.1562	1.8204	0.0125	2.1621
13	0.1533	1.8212		
14	0.1505	1.8220		
15	0.1480	1.8226		
16	0.1451	1.8234		
17	0.1421	1.8242		
18	0.1392	1.8250		
19	0.1362	1.8257		
20	0.1331	1.8265		

Note: The columns labeled Point 1 & Point 2 show the distance from the crack front to the surface of repaired weld.
Point 1 = outer extreme of the minor diameter of ellipse (closer to surface)
Point 2 = inner extreme of the minor diameter of ellipse (further from surface).

a,c,e

Figure C.3-1 Axial Crack in the Penetration J-Weld

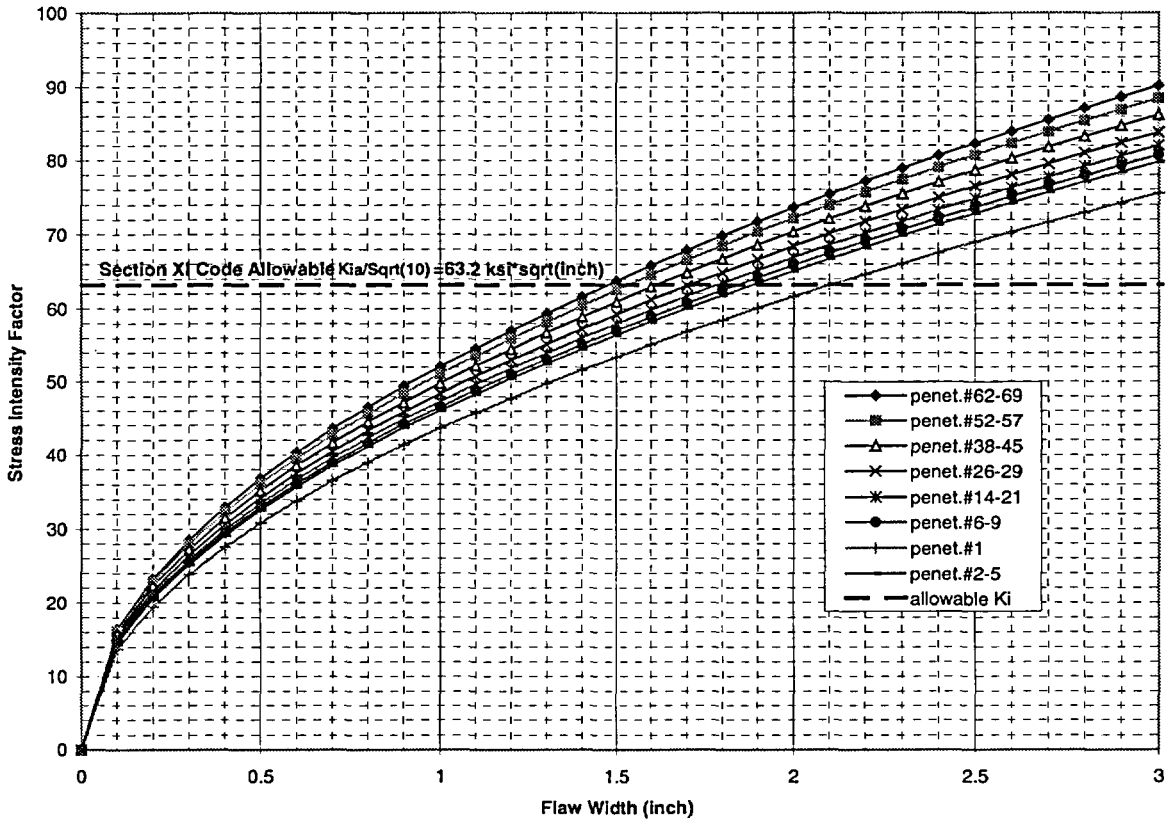

Figure C.3-2 Determination of Allowable Flaw Size (for Illustration Purposes Only)

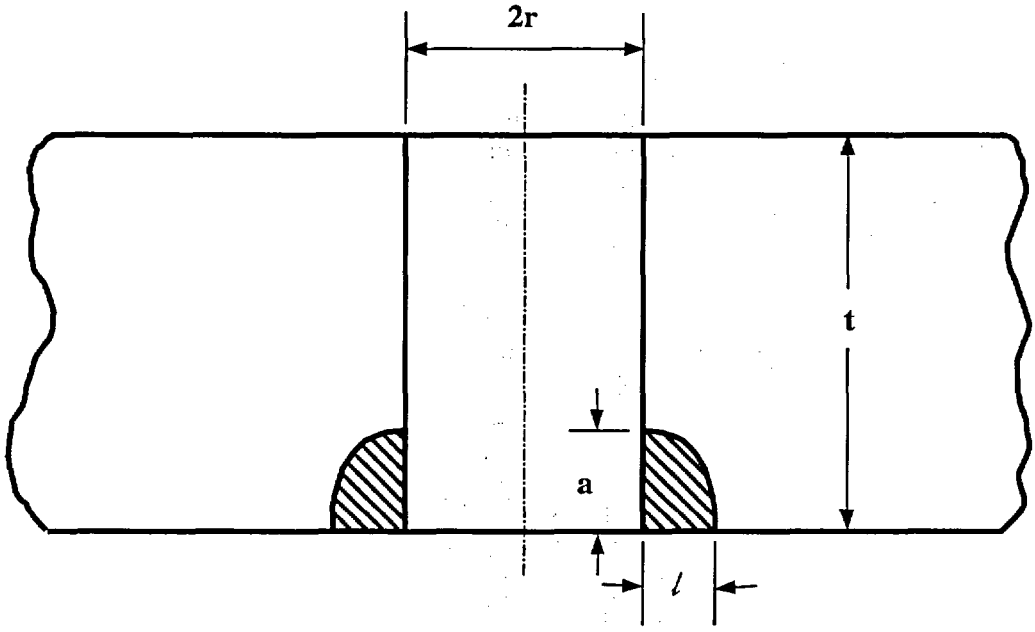

Figure C.3-3 Geometry and Terminology as Applied in [ ]^{a,c,e}

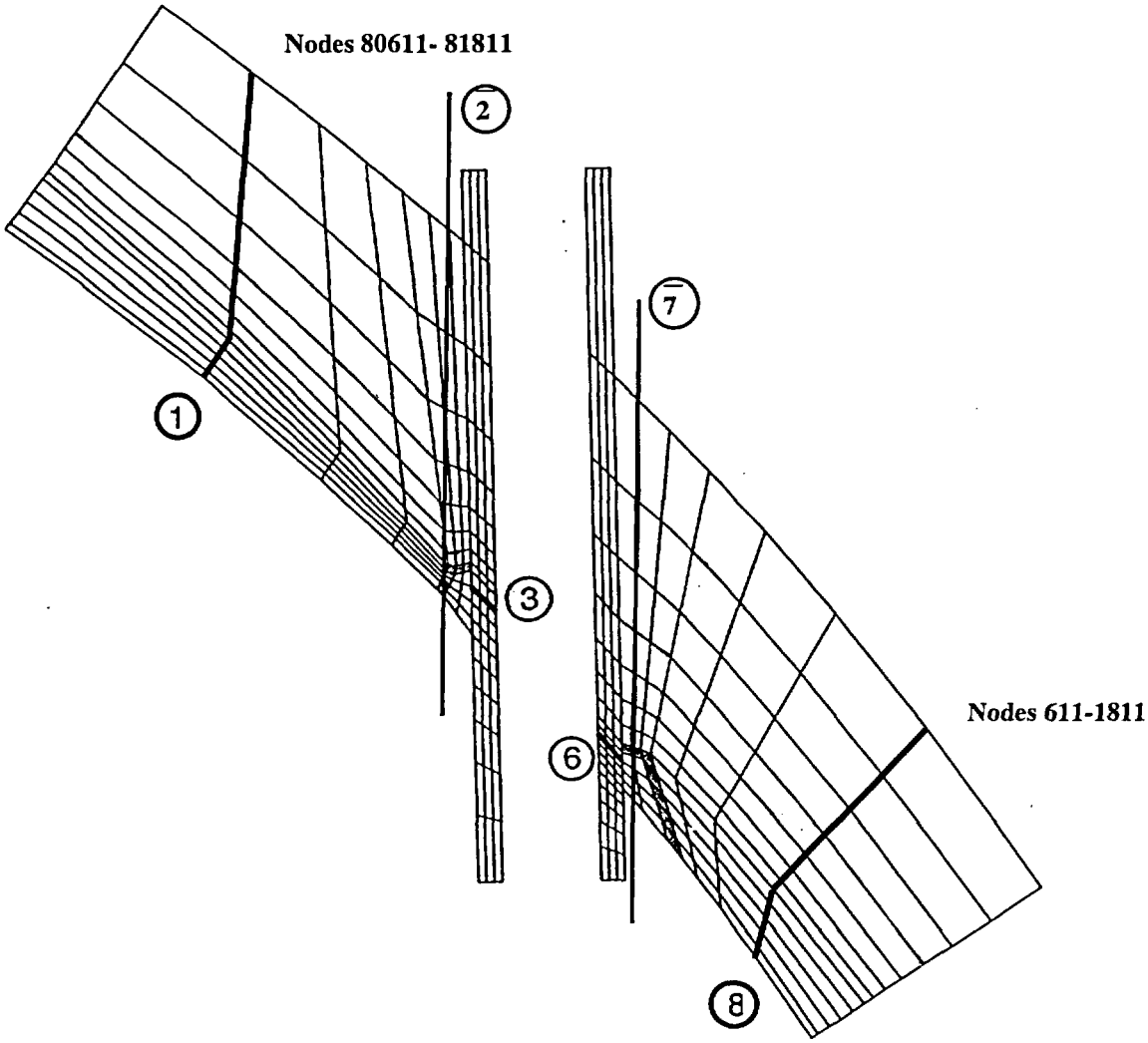

Figure C.3-4 Finite Element Model with Selected Stress Cuts

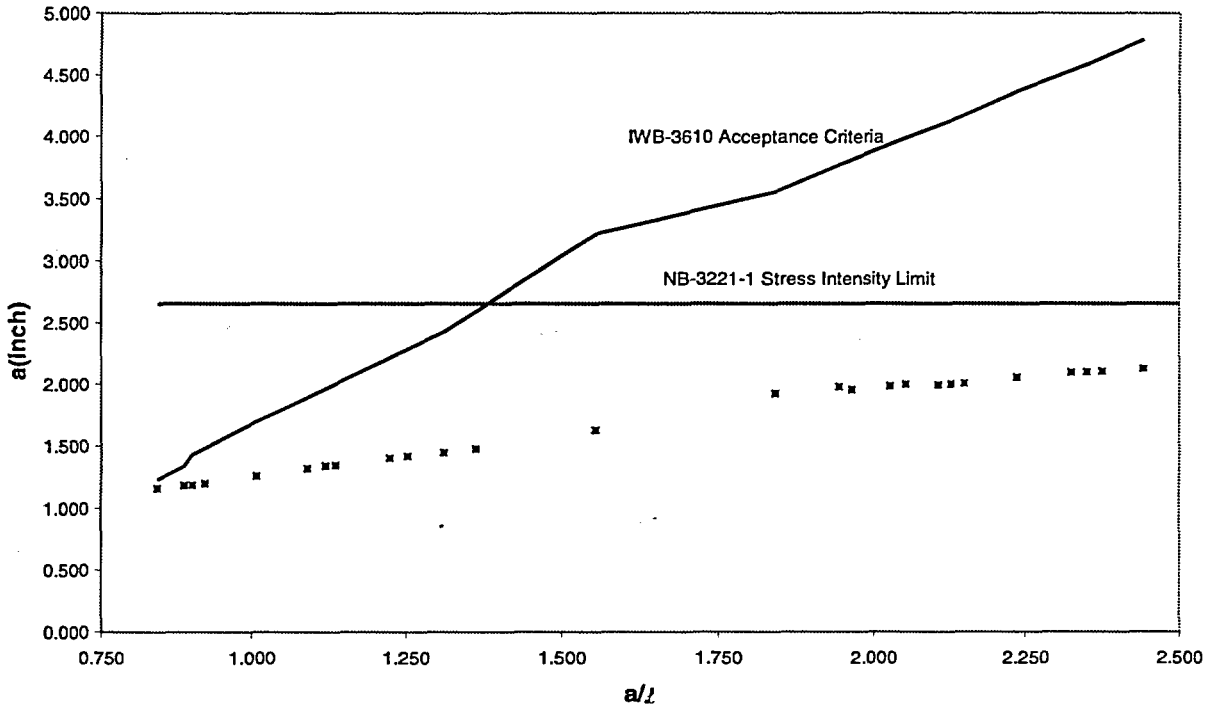

Figure C.3-5 Fatigue Crack Growth Adjusted Allowable Flaw Sizes for Head Penetration Attachment Welds (for Illustration Purposes Only)

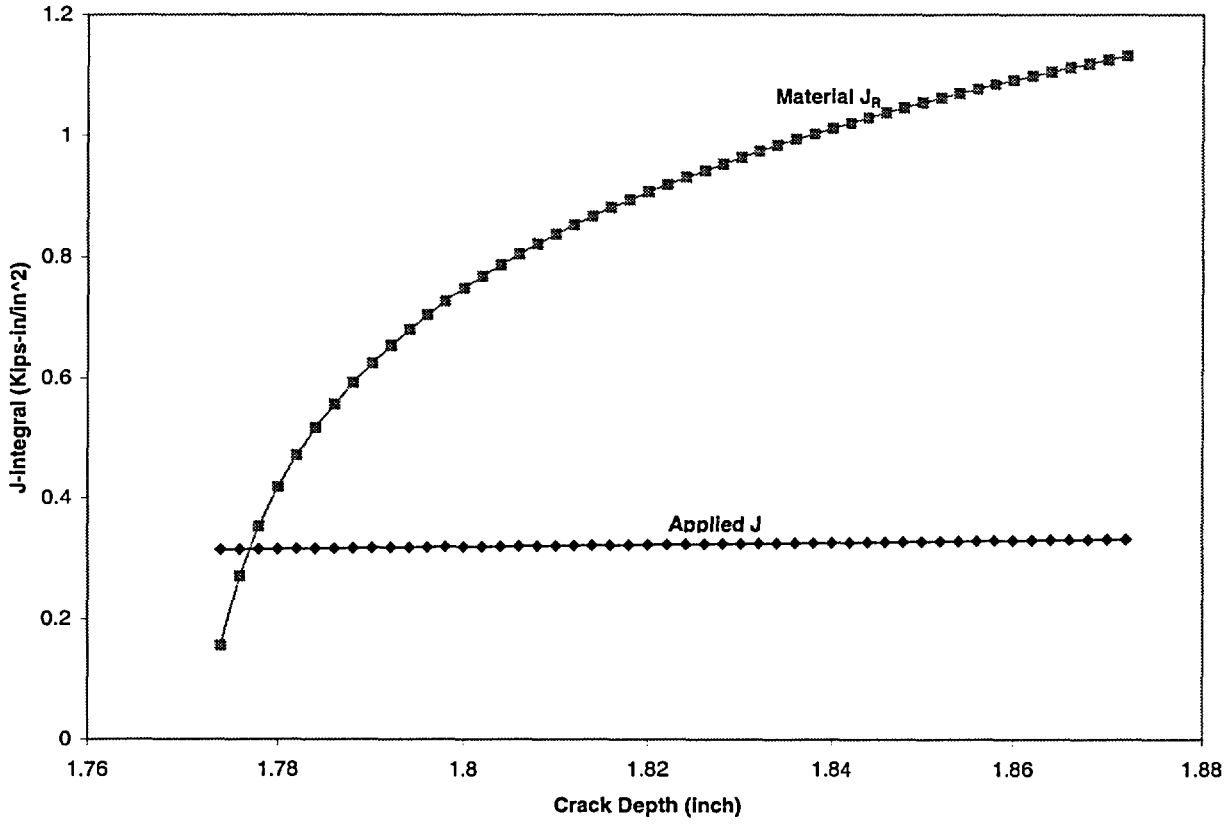

Figure C.3-6 Comparison of the Slope of the Applied J-Integral and J-R Curve (for Illustration Purposes Only)

C.4 SCENARIO # 3 - AXIAL CRACK ON THE PENETRATION TUBE OD (BELOW THE J-WELD)

[

]^{a,c,e} A crack in the OD of the tube (below the weld) is not an integrity concern, but it could be a leakage concern if it extends above the J-weld region. At this point the crack may compromise the vessel pressure boundary. Performing a weld overlay of the crack area will eliminate the potential pathway for primary coolant to escape the vessel.

C.4.1 Methodology

The evaluation assumed that a flaw has been detected in a penetration nozzle OD and that the embedded flaw repair method is used to isolate the flaw from further exposure to the primary water environment. The evaluation began with the determination of an allowable flaw size as discussed in Section C.4.2 for a flaw postulated in the penetration nozzle OD. [

]^{a,c,e} The reduced allowable flaw size was then used as the maximum allowable flaw size that can be tolerated using the embedded flaw repair method.

The evaluation procedures and acceptance criteria for indications in austenitic piping are contained in paragraph IWB 3640 of ASME Section XI [1]. [

]^{a,c,e}.

C.4.2 Allowable Flaw Size

The methodology used in determining the allowable flaw size is the same as that used for the axial flaw in Scenario #1. The allowable flaw sizes for a maximum design pressure of 2.5 ksi can then be determined as illustrated in Figure C.4-2 for a postulated outside surface axial flaw with a given aspect ratio (flaw length/flaw depth). Allowable flaw sizes determined from Figure C.4-2 must be adjusted to account for the fatigue crack growth of the repaired flaws, which are embedded and free from stress corrosion cracking. The amount of adjustments will be based on the fatigue crack growth analysis described in Section C.4.3.

C.4.3 Fatigue Crack Growth Prediction

The methodology used in determining ΔK_I is the same as that used for the axial flaw in Scenario#1 except that the crack growth is calculated for an outside axial surface flaw instead of an embedded flaw.

Stress Intensity Factor for Surface Flaw

For a part-through wall flaw, the stress profile is approximated by a cubic polynomial as follows:

$$\sigma(x) = A_0 + A_1 x + A_2 x^2 + A_3 x^3$$

where:

x	=	The Distance into the wall (inch)
σ	=	Stress Perpendicular to the plane of the Crack (ksi)
A_i	=	Coefficients of the Cubic Polynomial Fit, i = 0, 1, 2, 3

For a surface flaw in the penetration nozzle, the stress intensity factor expression of Raju and Newman [2] is used as discussed in Section C.2.3.3.

Once ΔK_I is calculated, the fatigue crack growth due to a particular stress cycle can be determined using a crack growth rate reference curve applicable to the material of the head penetration nozzle. [

]^{a,c,e}

Once the incremental crack growth is calculated, it is then added to the original crack size, and the analysis proceeds to the next cycle and/or thermal transient. The procedure is repeated in this manner until all the significant analytical thermal transients and cycles known to occur in the 10, 20, 30 or 40 years of operation have been analyzed. The cycles are distributed evenly over the entire plant design life.

C.4.4 Maximum Allowable Flaw Size

Allowable flaw sizes determined as discussed in Section C.4.2 were adjusted to account for the fatigue crack growth of the repaired flaws, which are embedded and free from stress corrosion cracking. These embedded flaws are the result of repairing the axial part-through flaws on the outside surface of the penetration nozzles using the embedded flaw repair method. The amount of adjustments is based on the fatigue crack growth analysis result described in Section C.4.3.

Maximum Allowable Flaw Sizes for Embedded Axial outside Surface Flaws

Figure C.4-3 illustrates the maximum allowable flaw sizes for the embedded axial outside surface flaws in the head penetration nozzles along with the ASME Code based allowable flaw depths and shapes discussed in Section C.4.2. The results have incorporated the effects of fatigue crack growth.

a,c,e

Figure C.4-1 Axial Crack on the Penetration Tube OD (Below the J-Weld)

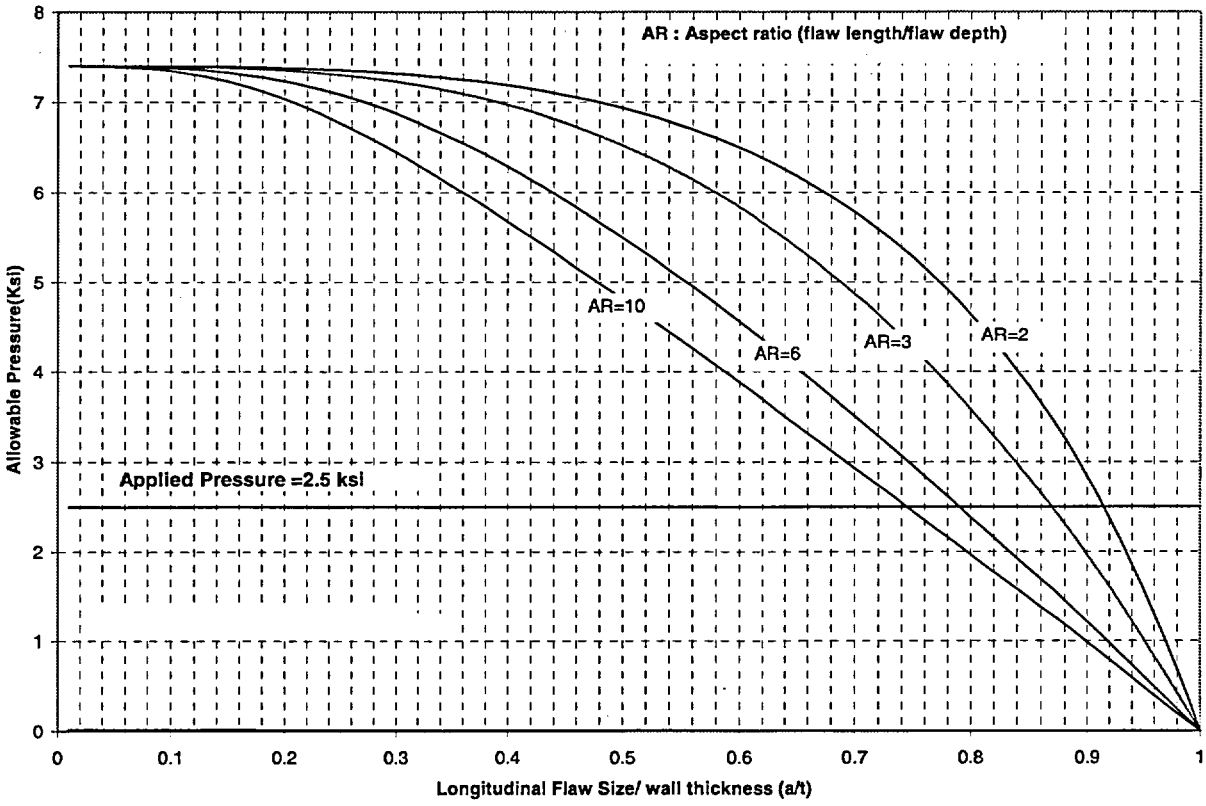

Figure C.4-2 Determination of Allowable Axial Outside Surface Flaw Sizes (For Illustration Purposes Only)

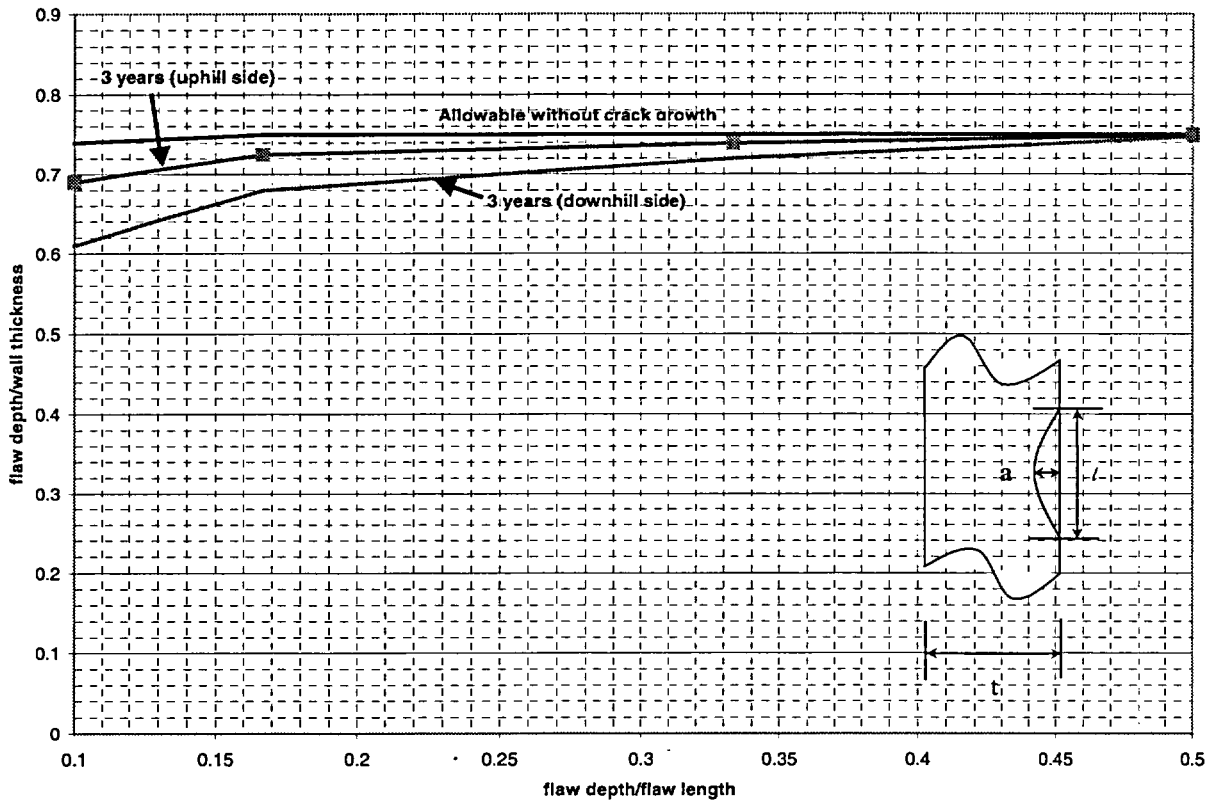

Figure C.4-3 Maximum Allowable Embedded Axial Outside Surface Flaw sizes (for Illustration Purposes Only)

C.5 REFERENCES

1. ASME Code Section XI, "Rules for Inservice Inspection of Nuclear Plant Components," 2001 edition, 2002 Addendum.

2. Newman, J. C. and Raju, I. S., "Stress Intensity Factor Influence Coefficients for Internal and External Surface Cracks in Cylindrical Vessels," in Aspects of Fracture Mechanics in Pressure Vessels and Piping, PVP Vol. 58, ASME, 1982, pp. 37-48.

3. NUREG/CR-6721 ANL/01/07 "Effects of Alloy Chemistry, Cold Work, and Water Chemistry on Corrosion Fatigue and Stress Corrosion Cracking of Nickel Alloys and Welds" Date Published: April 2001

4. [

]^{a,c,e}

5. Marston, T.U. et al., "Flaw Evaluation Procedures: ASME Section XI," Electric Power Research Institute Report EPRI-NP-719-SR, August 1978.

6. "Development of Criteria for Assessment of Reactor Vessels with Low Upper Shelf Fracture Toughness," Welding Research Council Bulletin 413, July 1996.

7. Regulatory Guide 1.161, "Evaluation of Reactor Pressure Vessel with Charpy Upper-Shelf Energy Less than 50 ft-lb.", June, 1995.